BEN-GURION UNIVERSITY OF THE NEGEV
FACULTY OF ENGINEERING SCIENCES
DEPARTMENT OF ELECTRICAL AND COMPUTER ENGINEERING

SIGNAL AND PATTERN GENERATION FOR MUSCLE MANIPULATION IN MEDICAL APPLICATIONS

THESIS SUBMITTED IN PARTIAL FULFILLMENT OF THE REQUIREMENTS
FOR THE MSc. DEGREE

By: Hagit Perets Habany

Supervised by:
Prof. Mor Mordechai Peretz

October 2019

BEN-GURION UNIVERSITY OF THE NEGEV
FACULTY OF ENGINEERING SCIENCES
DEPARTMENT OF ELECTRICAL AND COMPUTER ENGINEERING

SIGNAL AND PATTERN GENERATION FOR MUSCLE MANIPULATION IN MEDICAL APPLICATIONS

THESIS SUBMITTED IN PARTIAL FULFILLMENT OF THE REQUIREMENTS
FOR THE MSc. DEGREE

By: Hagit Perets Habany

Supervised by:
Prof. Mor Mordechai Peretz

Author:	Hagit Perets Habany	…….	Date: 06.10.19
Supervisor:	Prof. Mor Mordechai Peretz	…….	Date: 06.10.19

Chairman of graduate studies committee:

Name: …… ……. Date: 04.02.2020

October 2019

Abstract

This thesis addresses signal and pattern generation for transcutaneous muscle manipulation in medical application. The work mainly covers airway obstruction problem, a life threatening condition of respiratory blockage which currently being treated mostly in non-electrical approach, which suffers from problematic drawback of speed limitation. The primary aim of this thesis is to design and implement a portable sinusoidal current generator with suitable signal patterns to initiate relaxation of the muscle responsible for breathing channel and maintain it relaxed for the time procedure duration, while obtaining safe operation to both the applicator and the subject at all time.

One objective of this thesis is to introduce a sinusoidal current generator for muscle manipulation application. In electrical nerve excitation application, the current is transfer normally through encircling nerve cuff electrodes, which is an invasive approach and unpractical in case of airway blockage trauma. Therefore, by operating a transcutaneous muscle manipulation generator, the cuffed electrodes could be replaced by external electrodes that placed on the skin and the generator could be used quickly in both life threatening situation and routine procedures as well. To reach this goal, this work presents a two- stage current sourcing sinusoidal generator, to drive a nonlinear load, such as the human body through the skin and other tissues. The research includes introduction of the electrical nerve excitation and challenges regarding through-skin operation, detailed architecture of the proposed system, principle of operation of resonant converters and two stage resonant converter, current sensing approach of the output current amplitude, control algorithm, practical implementation, human interface, safety aspect and experimental results of the system preliminary prototype that was built and evaluated.

Another objective of this thesis is to create a unique signal patterns suitable to excite nerve blocking in quick and reversible manner. Due to uncertainty regarding the specific parameters required to achieve the desired flaccid paralysis, the generator features separately adjusted output current amplitude, time duration pulse and switching frequency.

Most of the research has been published in the proceedings of the IEEE Applied Power Electronics Conference and Exposition (APEC) 2019 [1]

Acknowledgments

I would like to thank my supervisor Prof. Mor Mordechai Peretz with whom I worked for the last three years. His excellent guidance and support led me to absorb a great satisfaction from our work and accomplishments. Prof. Peretz has impelled me to excellence, providing me with the opportunities for enjoyment and for the self-fulfillment of achieving my goals.

I want to thank Dr. Michael Evzelman for being a supportive tutor and a friend over the last two years. I thank him for his tremendous help, collaboration, and ideas.

I must not forget all my colleagues at the Center for Power Electronics and Mixed-Signal IC, whose support and friendship meant so much: Dr. Alon Cervera, Mr. Tom Urkin, Mr. Bar Halivli, Mr. Doodi Dayan, Mr. Guy Sovik, Mr. Alex Mindel, Mr. Erez Masandilov, Mr. Eli Abramov and anyone that I have forgotten to mention by name.

Of the technical staff, I would like to thank Mr. Azrikam Yehieli, who is responsible for the excellent working and social conditions of the laboratory.

With great appreciation I thank my husband Sahar, for his tremendous loving support, patience and care. I want to thank my parents and sisters for their support and care along this challenging path.

Last but not least, I would like to thank the funds that supported my research: The Israeli Ministry of Science and Technology MOST, without whom the research could not have been conducted.

Table of Contents

Figures List

Tables List

Acronyms and Abbreviations

IV – Intravenous
KHFAC – Kilo-hertz frequency alternating current
KES – Kilohertz Electrical Stimulation
ZCS – Zero-current switching
ZVS – Zero-voltage switching
HB – Half bridge
FB – Full bridge
THD – Total harmonic distortion
HPF – High pass filter
LPF – Low pass filter
ADC – Analog to Digital Converter
PWM – Pulse width modulation
MCU – Microcontroller unit
FFT – Fast Fourier Transform

Inline References Legend

X.XX – Chapter / Section number
(X.XX) – Equation
[XX] – Reference
Fig. X.XX – Figure

1. Introduction

1.1. Motivation

1.1.1. Airway Obstruction

Airway obstruction is the overall name for blockage in any part of the respiratory system. The blockage can be partial or complete, in both cases preventing air to flow into the lungs.

Among some of the causes to airway obstruction are allergic reaction, penetration of foreign object to the throat and laryngospasm, which is an involuntary muscular spasm of the muscles in the upper airway.

Laryngospasm is a protective reflex designed to prevent foreign object entering the throat. It should be known that anesthesia can trigger this reflex as well. In normal cases, the blockade due to laryngospasm can lasts for about one minute, but for anesthesia as trigger, the obstruction can last longer.

Due to the causes outlined above, there is a hazard of chocking or complete airway blockade. Moreover, in case the blockade is not treated immediately and rapidly, it may result in life threatening consequences such as cardiac arrest, gastric aspiration, pulmonary edema and arrhythmia [2].

Therefore, in order to maintain open airway by performing intubation (insertion of flexible tube into the trachea) and ventilation, muscle relaxation is necessary.

The common practice today to achieve channel opening is by using intravenous (IV) medications treatment.

1.1.2. IV medications

As for today, muscle relaxation for airway management is performed by the administration of IV medications, which allow flaccid paralysis for fixed amount of time, regardless the desired time, often more time than needed. There are several drawbacks to IV medication, as detailed in the following list.

1. Side effects: Among the common side effects of IV medications are high blood levels of potassium, low blood pressure, muscle pains, cardiac arrest and various neurologic damage [3]. This collateral damage may be even more dangerous and life threatening than the original airway obstruction condition, an important fact taken into consideration in medical decisions.

2. Speed limitation of onset and offset operation: Rapid securement of the airway path is the most important goal while treating a patient. One of the shortest acting IV muscle relaxants may require 20 minutes for offset and 90 seconds for onset [4]. This valuable time may be the difference between health, neurologic damage or even death.

3. Contraindications and adverse reactions to IV muscle relaxation: Among all the medications given intravenous, IV muscle relaxants have the highest incidence of anaphylactic, which is allergic reaction to an antigen [5].

4. Requirement of vein access: Performing vascular access procedure is causing an additional delay to the entire process of airway opening.

These limitations cause delay in airway opening, in some cases their usage is prohibitive and in critical cases can cause a permanent neurologic injury or even death from hypoxia – which is oxygen deficiency in body tissue [6].

1.2. Electrical nerve excitation

A better alternative approach to IV medication for airway management is by using electrical nerve excitation to relax the muscle responsible for breathing channel.

The use of electricity for control of the nervous system has been an established tool in medicine for many years now [7].

In general, an electrical pulse can produce an action potential in a neuron that, once it spreads out, is identical to a normal, physiologically generated action potential. This feature makes electrical stimulation a powerful control tool of the nervous system within the body, for various medical applications.

Many researches were conducted in order to investigate which electrical waveforms are the ones desired to create in order to block or inhibit action potential propagation.

Introduction

The most commonly used method today for reversible electrical nerve conduction block is known as Kilo-Hertz Frequency Alternating Current (KHFAC) [8] or Kilohertz Electrical Stimulation (KES) [9], when they both refer to the same phenomena.

KHFAC was first introduce in 1935 [10] and since then was demonstrated in a variety of animal models, including frogs [11] - [13], rats [14] - [16], and others [17] - [23]. These studies have demonstrated the ability to achieve a quick, reversible, localized block of peripheral nerve activity.

There are some unique characteristics to KHFAC. A summary of the main features is detailed below:

1. Frequency: Based on previous studies, in order to achieve nerve conduction block a minimum frequency of 1kHz is required [15]. Nevertheless, more commonly to find 5kHz as the lowest frequency used. As for maximum frequency, up to 70kHz was reported as effective experimentally [14] and up to 100kHz have been evaluated in theory research [24].

2. Amplitude: KHFAC amplitude is typically reported as current (mA) or voltage (V), where there is a minimum amplitude requirement at a given frequency, referred to as 'block threshold', for production of complete block at the targeted nerve [25].
   It was found that the amplitude increase linearly as the frequency increase, over the range of 5 – 30kHz [12], [15], [17], [23], [26].
   Moreover, KHFAC block has a useful feature – the percentage of the nerve blocked could be modulated by changing the waveform amplitude [25] , therefore achieving partially block muscle activity while retaining some voluntary muscle function.
   It should be noted that low amplitude KHFAC waveforms could produce repetitive firing in the nerve.

3. Electrodes: In order to apply KHFAC block to certain area only, an implanted encircling nerve cuff electrodes are normally used, as can be seen in Fig. 1.1. In this way, a localized block of the desired nerve is achieved without affecting other body areas. However, this approach is invasive and unpractical in trauma events.

(a) (b)

Fig. 1.1 Standard nerve cuff electrode. (a) Typical nerve cuff electrode. (b) Illustration of nerve cuff electrode with peripheral nerve

4. Onset response: When initiating KHFAC, there is a short duration of increment in nerve activation, named ‘onset response’ [25], [27]. The onset response can be a large ‘twitch’ response, or a period of sustained activity.

   The motor onset response can be divided into two phases: first phase is the muscle twitch which always occurs, followed by the second phase which is period of repetitive firing that ends with complete or partial block that can be reduced by electrodes and waveform optimization [27], [28].

5. Effects on neural responses: KHFAC stimulator generates a variety of nerve responses such as blocking, reversing and more, as a function of current or voltage amplitude, frequency and pulse duration of delivery. Each of these parameters effects on the accepted nerve block / activation.

   In Fig. 1.2 a comparison between KHFAC stimulator and standard low frequency stimulator from [8] is presented.

   As can be seen, the responses of KHFAC are much complicated than the low frequency stimulator. Also, there is a need for additional investigation in order to fully understand the transitions between these known states. Moreover, it is unaware if the presented states are the final number of states, or perhaps there are more unknown states.

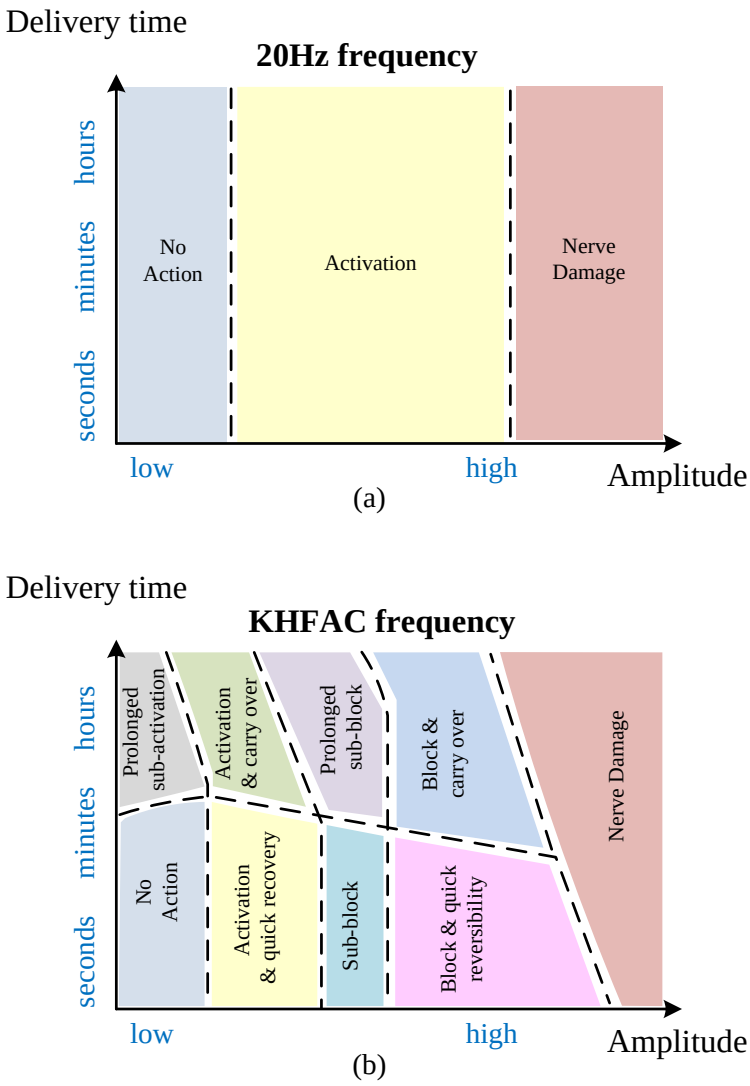

Fig. 1.2 Comparison between low and high frequency stimulation presented in [8], considering the effect of amplitude and delivery time. (a) A 20Hz frequency stimulation with three known effects on the nerve: no nerve action, nerve activation and nerve damage. (b) KHFAC stimulation with at least nine possible known effects: no nerve action, prolonged sub-activation, activation & quick nerve recovery, activation & carry over, sub nerve block, prolonged sub-block, block & quick nerve reversibility, block & carry over and nerve damage.

1.3. Benefits of electrical nerve stimulation

Among the unique characteristics of electrical nerve stimulation, as detailed in chapter 1.2, there are two key features that distinguish it from other non - electrical methods of nerve block, as detailed below.

1. Instantaneous activation and deactivation of nerve block operation: Electrical nerve block occurs almost instantly. The typical duration is less than 2 seconds [25], while for KHFAC nerve block the duration is less than 10 millisecond [29]. Comparing it to IV medication, detailed in chapter 1.1.2, electrical nerve block occurs far more rapidly.

In [29] there was use in counted cycles method in order to measure the amount of time needed to complete motor block and it was found to be in the range of 7.5 to 14 millisecond.

2. Reversibility: After the KHFAC nerve block terminate its operation, the nerve recovers completely and return to normal activity rapidly. For example, in [25] complete recovery of the nerve occurs within one second of the cessation of the KHFAC.

These two important features allow conducting and reversing the nerve in a fast and secure manner, which can be very useful in case of medical emergency in general and airway management in particular.

1.4. Objectives and significance of the research program

1.4.1. Primary hypothesis and innovation

As mentioned in section 1.2, encircling nerve cuff electrodes are normally used today in order to apply electrical nerve block stimulation for various applications.

For example, in [17] electrical nerve block is used to control the pudendal nerve (the main nerve of the perineum which supply motor activity to the sphincter muscle responsible for urination) in order to provide a treatment for restoring urinary voiding for patients with bladder–sphincter dyssynergia.

Unfortunately, although this type of electrodes has been proven as effective for electrical nerve block, they are invasive and not suited for airway management treatment, especially in case of trauma.

This leads to the innovation of this research, which is to design and implement a portable sinusoidal current generator for transcutaneous muscle application, by replacing the cuffed electrode with external noninvasive electrodes. The external electrodes will deliver a shaped charge to the airway nerves through the skin, thereby relaxing the relevant muscle.

The primary hypothesis is that flaccid paralysis of the nerve could be achieved via external non-invasive application of nerve stimulation, as oppose to current solutions. The device, as presented in Fig. 1.3, would be most valuable in case of critical situation where quick airway management is needed.

Moreover, due to its advantages over IV medication, such as quick activation and deactivation, the device could be in use for routine procedures as well as for other medical application

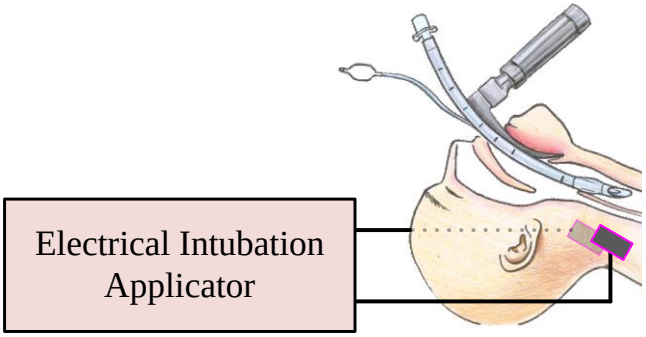

Fig. 1.3 Abstract representation of the generator and the subject of application

1.4.2. Challenges of transcutaneous muscle manipulation

There are some challenges needs to be taken into consideration when designing transcutaneous nerve excitation using electrical current.

First, is the non-linear behavior of the human skin, as can be seen in Fig. 1.4. In a normal, non-conducting state, the impedance of the human skin is considered high, in the range of several kilo-ohms. However, once conduction path is induced, the skin impedance drops to several hundred ohms [30].

When constant current amplitude is desired during the entire conduction process, this behavior could be problematic and should be taken care.

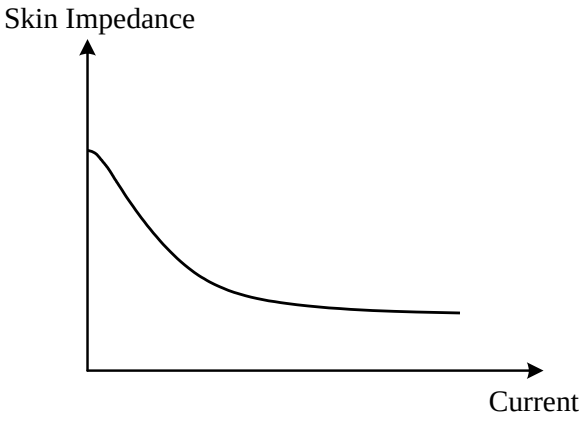

Fig. 1.4 Skin impedance non-linear behavior

Another challenge is associated to the different current amplitude required to relax the muscle and to maintain it relaxed, as can be seen in Fig. 1.5b.

A higher current is required to initiate muscle relaxation, due to the high impedance of the skin in this state, while a much lower current is needed to maintain the flaccid paralysis.

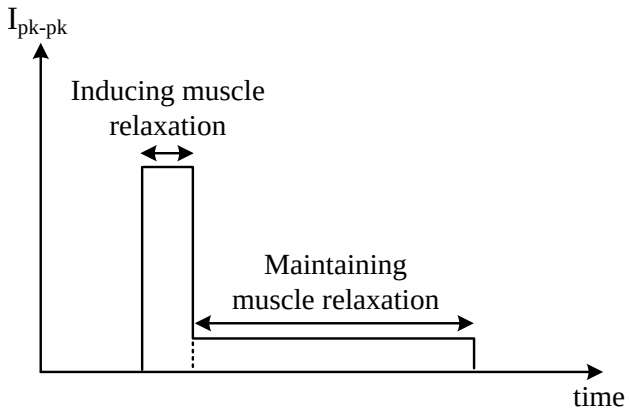

Fig. 1.5 Current pattern generation for initiating nerve block with high amplitude and continuing nerve block with low amplitude

The last challenge is the aspect of safety operation, to both the patient and the applicator during the entire operation time.

One issue of safety is charge count and total charge parameters validation in order to avoid tissue damage by accumulation of charge on the skin.

Another issue is designing a current path in order to verify that current flow solely through the subject so there is no electrocution hazard for the applicator.

2. Resonant Converter

2.1. Background

In order to comply with the system requirements for high frequency sinusoidal current, there are several ways to convert DC input voltage, such as power supply or battery, into AC current, in particular sinusoidal wave. Moreover, in standard modern electronic systems, there is a demand for small, high quality, power efficient, lightweight and reliable electronic [31] - [35].

There are numerous methods to create sinusoidal current source. A common one is by using feedback oscillators (general block diagram in Fig. 2.1) such as Wein Bridge [36], Hartley or Colpitts [37].

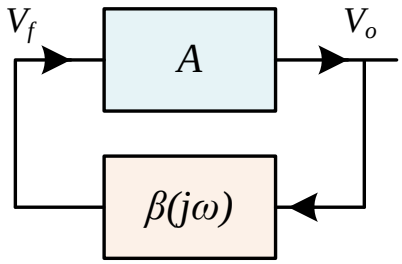

Fig. 2.1 Block diagram of general feedback oscillator with sinusoidal output voltage V_o , an electronic amplifier A, build from transistor or op-amp and feedback network $\beta(j\omega)$ constructed from resistors, inductors and capacitors.

Although producing virtually pure sinusoidal waveform, they have a major disadvantage – their frequency is determined by the system passive components and cannot be programmable as desired.

Another option is H- bridge inverter [38] such as DC -AC Buck / Buck - Boost inverter. In this type of inverter, the output voltage frequency is determined by the sinusoidal duty cycle frequency, named the fundamental frequency, which has to be much lower than the switching frequency in order to allow stable system. As a result, this type of inverter is suitable mainly for low frequency sinusoidal waveform, as oppose to the necessity in this specific application.

The commonly used method today for high frequency sinusoidal waveform is resonant converter [39], as will be explain extensity in the following chapter. This method is

suitable producing sinusoidal waveform in high frequency. Due to the high switching frequency, the size of the resonant component is smaller, allowing the system to be small and lightweight.

2.2. First Harmonic Approximation

Resonant converter can be divided into two fundamental parts[40]: controlled switching network and resonant tank network, as shown in Fig. 2.2.

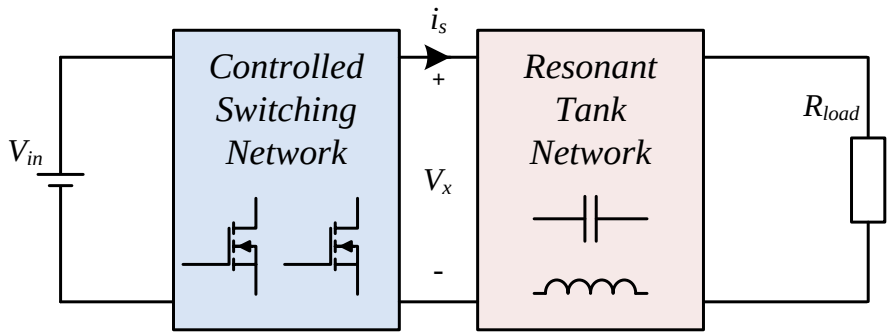

Fig. 2.2 Abstractive representation of general resonant converter system consisting control switching network and resonant tank network

When operating resonant converter, the controlled switching network produces a square wave output voltage $V_x(t)$ that can be expressed by the Fourier series (2.1 equation is for $D = 50\%$). $V_x(t)$ may consist a DC component, in case of half bridge switching network, or without DC component in case of full bridge switching network.

$$V_x = \frac{4}{\pi} V_{amp} \cdot \sum_{n=1,3,5\ldots}^{\infty} \frac{1}{n} \sin(2\pi n f_{sw} t) + (\frac{V_{in}}{2}) \qquad (2.1)$$

If the switching frequency f_s is designed to be in the vicinity of the resonant frequency f_r, $f_s \approx f_r$, and the resonance tank contain high quality factor Q at f_s than the resonant tank rings with approximately sinusoidal waveform on frequency f_s.

These can be understood by the frequency spectrum shown in Fig. 2.3 , where the low pass / band pass characteristics of the resonant tank filter all the other harmonics of the square wave - nf_s, $n=3,5,\ldots$ except the fundamental component (2.2) when n=1.

$$V_x = \frac{4}{\pi} V_{amp} \cdot sin(2\pi f_{sw} t) \qquad (2.2)$$

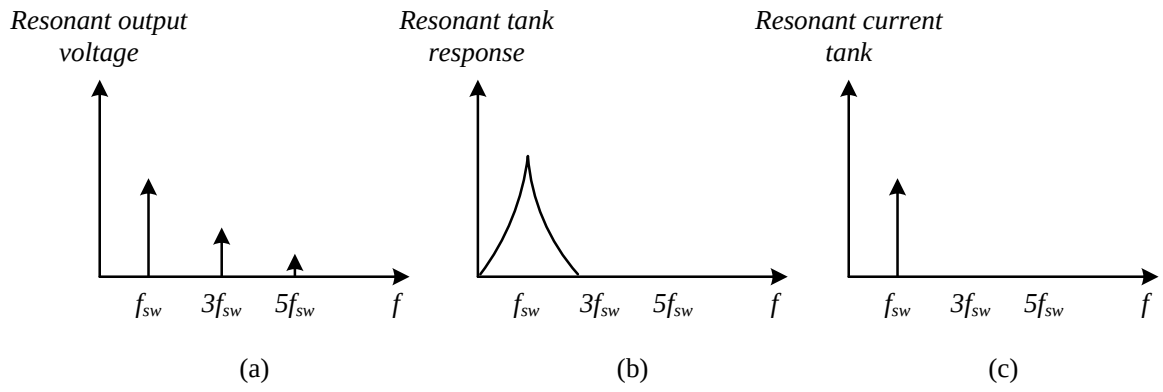

Fig. 2.3 Frequency spectrum of (a) Square wave output voltage V_x (b) Resonant tank transfer function, high Q around $f_s \approx f_r$ (c) Tank current i_s with the fundamental component only

This sinusoidal approximation allows simple equivalent circuits to be derived - sinusoidal voltage source instead of square wave source for the bridge inverter. Moreover, for the equivalent circuit the operation is well understood and can be solved using simple linear AC analysis, as detailed in the following chapter.

2.3. Types of Resonant Converter

2.3.1. Background

As presented in chapter 2.2, in order to understand properly the operation of resonant converter the first harmonic approximation was introduced. By using this approximation, a simple equivalent circuit constructed from sinusoidal voltage source can be derived, as can be seen in Fig. 2.4.

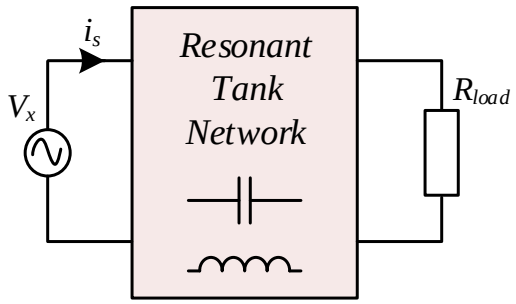

Fig. 2.4 An equivalent resonant converter circuit using the sinusoidal approximation

Moreover, there are two main controlled switching networks: half bridge (HB) network and full bridge (FB) network as can be seen in Fig. 2.5, where the operation on both is by switching the network switches S_H and S_L in a complementary manner.

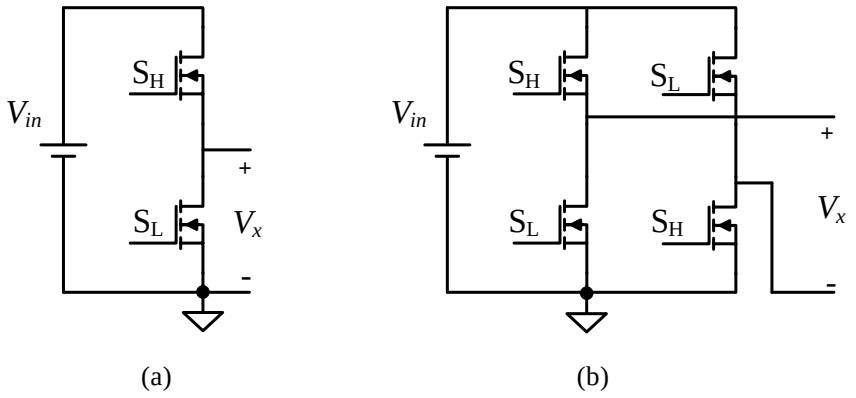

Fig. 2.5 Two controlled switching network (a) Half bridge network (b) Full bridge network

For each one of the networks there is different influence on V_x by the amplitude and by the DC component, as described in (2.3) and (2.4).

$$V_{x\_HB} = \frac{2}{\pi} V_{in} \cdot sin(2\pi f_{sw} t) + \frac{V_{in}}{2} \quad (2.3)$$

$$V_{x\_FB} = \frac{4}{\pi} V_{in} \cdot sin(2\pi f_{sw} t) \quad (2.4)$$

As for the different resonant tank network, this summary will focus on three main types: series resonant converter, parallel resonant converter and series resonant parallel loaded converter [41]. All the equation that will be presented are for HB but suited for FB as well, under the consideration of (2.3) and (2.4).

2.3.2. Serial resonant converter

In series resonant converter the input voltage is consider to be sinusoidal as detailed in chapter 2.2 and the inductor is in series with the capacitor and output load (equivalent circuit in Fig. 2.6).

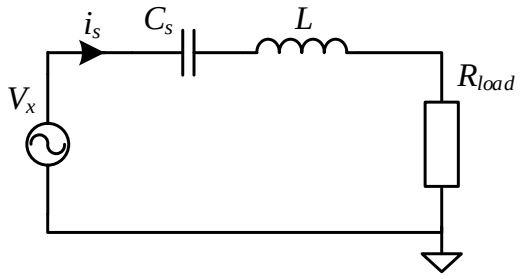

Fig. 2.6 A series resonant converter equivalent circuit

The transfer function from the input $V_x(s)$ to the output voltage $V_o(s)$ (2.5) is compatible with second order band pass filter (BPF) behavior (2.6), where Q_s is the quality factor of series converter (2.7) and ω_0 is the resonant frequency (2.8).

$$\frac{V_o}{V_x}(s) = \frac{sR_LC_s}{S^2LC_s+sR_LC_s+1} \quad (2.5)$$

$$H_{BP}(s) = \frac{\frac{s}{Q\omega_0}}{\frac{S^2}{\omega_0^2}+\frac{s}{Q\omega_0}+1} \quad (2.6)$$

$$Q_s = \frac{1}{R_L}\sqrt{\frac{L}{C_s}} \quad (2.7)$$

$$\omega_o = \frac{1}{\sqrt{LC}} \quad (2.8)$$

There is a requirement of virtually pure sinusoidal waveform by filtering all the harmonics. As a result, the system features low total harmonic distortion (THD) and a high - quality factor *Q* is needed.

For the airway management application, where the range of frequency is high in order to excite the nerve and the output resistance is high, a very high inductance *L* is required to achieve reasonably high *Q,* which in turn translates into a physically large inductor size (2.7), an unwanted situation for our application.

2.3.3. Parallel resonant converter

In parallel resonant converter, the inductor is placed in parallel with the capacitor and output load (equivalent circuit in Fig. 2.7).

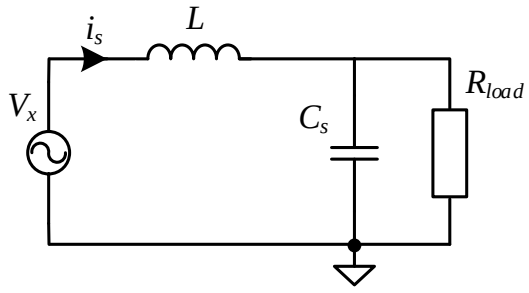

Fig. 2.7 A parallel resonant converter equivalent circuit

The transfer function from $V_x(s)$ to the output voltage $V_o(s)$ (2.9) is compatible with second order low pass filter (LPF) behavior (2.10), where the resonant frequency ω_0 is the same as the series resonant (2.8) but the quality factor Q_p is reversed (2.11).

$$\frac{V_o}{V_x}(s) = \frac{1}{S^2LC_s+s\frac{L}{R_L}+1} \quad (2.9)$$

$$H_{BP}(s) = \frac{1}{\frac{S^2}{\omega_0^2}+\frac{s}{Q\omega_0}+1} \quad (2.10)$$

$$Q_p = R_L\sqrt{\frac{C_p}{L}} = \frac{1}{Q_s} \tag{2.11}$$

As oppose to series resonant converter, in this case, the quality factor Q_p is high for large resistance R_L, such as the human skin, and it is more suitable for airway management application.

Another analysis option for this converter is by applying Norton's theorem which transforms the circuit from Fig. 2.7 into parallel equivalent, as shown in Fig. 2.8 [42].

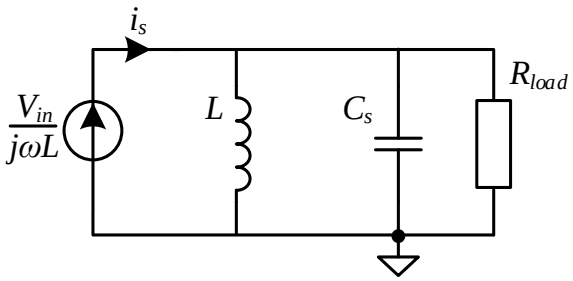

Fig. 2.8 An equivalent circuit using Norton's theorem

If working in the vicinity of the resonant frequency, than the impedance of the resonant network (L, C_s) is very high in comparison to the output load, thus all the current will flow into the output load, as described in Fig. 2.9.

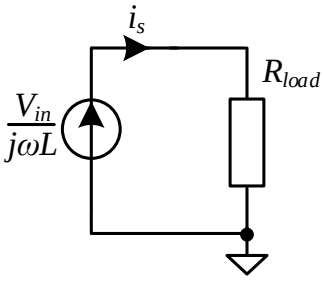

Fig. 2.9 An equivalent circuit using Norton's theorem for $f_s \approx f_r$

As a result, if working in the mentioned conditions, the circuit behaves as current source with different amplitude for every frequency.

However, there is DC component if using HB network. One possibility is by using FB network, which require additional hardware. Another option, used in this study, is series resonant parallel loaded converter.

2.3.4. Series resonant parallel loaded converter

In this case, the inductor is placed in series with the resonance capacitor, to which the load is connected in parallel (equivalent circuit in Fig. 2.10). The system also includes a blocking capacitor C_s that is intended to pass the AC current to the load while filtering out the DC component, in order to avoid DC currents. This capacitor is design to be much larger than the resonant capacitor, $C_s >> C_{res}$, thus his influence on the resonant network is negligibly small.

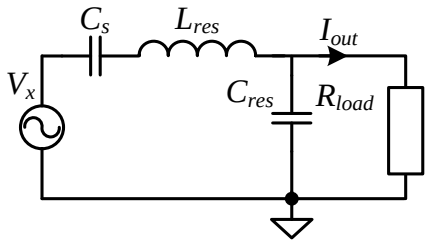

Fig. 2.10 A series resonant parallel loaded converter equivalent circuit

The full transfer function of the system (2.12) is complicated and difficult for understanding without simplification for different states.

Therefore, for low frequency when the inductor impedance is much lower than the capacitor impedance (2.13) while considering that $C_s >> C_{res}$, the system becomes a simple capacitor and resistor in series (Fig. 2.11).

$$\frac{V_{out}}{V_{in}} = \frac{sR_lC_s}{1+sR_l(C_s+C_p)+s^2LC_S+s^3LC_sC_pR_l} \tag{2.12}$$

$$Z_{C_s} \gg Z_L\,, \quad Z_{C_s} = \frac{1}{j\omega C_s},\ Z_L = j\omega L, \tag{2.13}$$

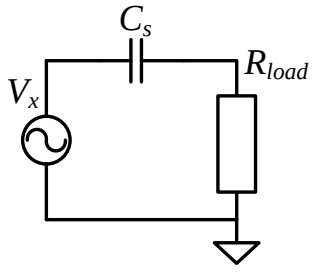

Fig. 2.11 An equivalnt circuit for series resonant parallel loaded converter in case of low frequency.

The transfer function becomes first order high pass filter (HPF) (2.14) with unity gain and known low frequency pole (2.15).

$$\left.\frac{V_{out}}{V_{in}}\right|_{low\ frequancy} = \frac{sR_lC_s}{1+sR_lC_s} \tag{2.14}$$

$$\omega_0 = \frac{1}{R_l C_s} \tag{2.15}$$

For high frequency, the inductor impedance is much higher than the capacitor impedance (2.16) than the circuit becomes the same as parallel resonant converter (Fig. 2.7) and the transfer function becomes second order LPF (2.17) around known resonant frequency (2.18).

$$Z_{C_s} \ll Z_L \tag{2.16}$$

$$\left.\frac{V_{out}}{V_{in}}\right|_{high\ frequancy} = \frac{1}{1+s\frac{L}{R_l}+s^2 L C_p} \tag{2.17}$$

$$\omega_0 = \frac{1}{\sqrt{LC_p}} \tag{2.18}$$

Since we designed the system under the restriction of $C_s >> C_{res,}$ than these two filters occurs in separate spectral frequency areas, when the relevant area for our application is the high frequency spectrum, as can be seen in Fig. 2.12.

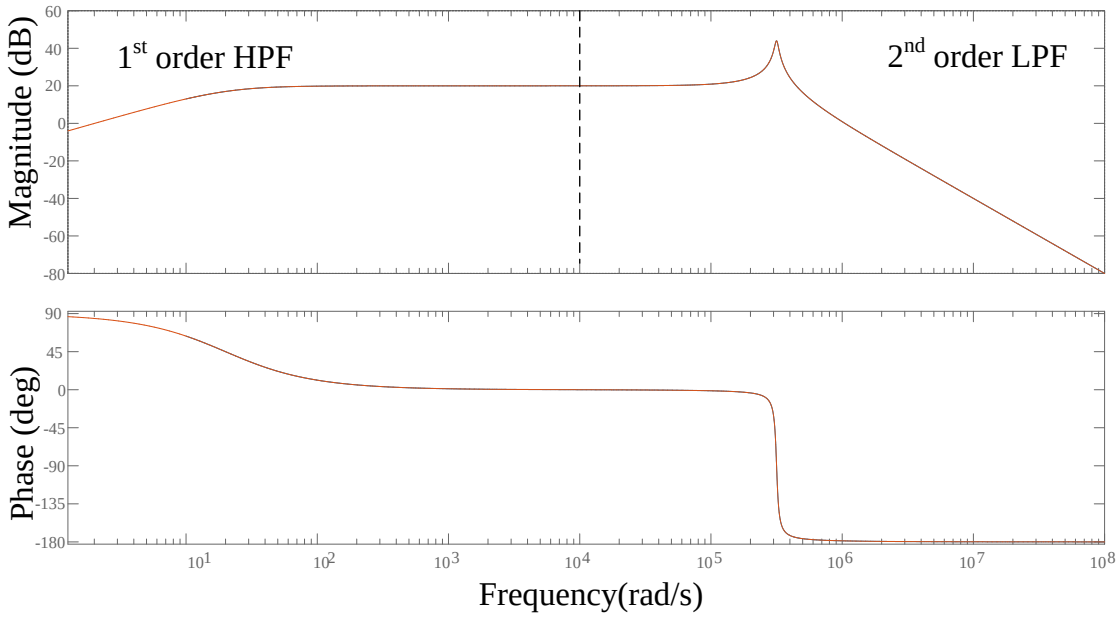

Fig. 2.12 Bode diagram of $V_o(\omega)$ in series resonant parallel loaded converter. On the left side, the system behaves like first order HPF. On the right side, the system behaves like second order LPF.

The approximated expression for output current amplitude in case of half bridge network is:

$$I_{out} = \frac{2V_{in}}{\pi \cdot R_{load}} \cdot \frac{1}{1+s\frac{L_{res}}{R_{load}}+s^2 L_{res} C_{res}} \tag{2.19}$$

It can be seen from (2.19) that the output current depends on both the input voltage V_{in} and the load R_{load}. Therefore, it should be taken into consideration that there is a problem maintaining constant output current for programmable frequency and variable output load.

2.4. Characteristics of resonant converters

2.4.1. Zero voltage switching and zero current switching

The main advantage of resonant converters is their reduced switching loss. This feature is possible due to the mechanisms known as zero-current switching (ZCS), and zero-voltage switching (ZVS).

When the resonant converter is operated below resonant frequency, $f_s < f_{res}$, the resonant tank presents a leading load to the switch network (Fig. 2.13) and the zero-current switching phenomenon can occur, in which the circuit causes the transistor`s current to go to zero before the transistor is turned off.

Similarly, when the resonant converter is operated above resonant frequency, $f_s > f_{res}$, the resonant tank presents a lagging load to the switch network (Fig. 2.13) and the zero-voltage switching phenomenon can occur, in which the circuit causes the transistor`s voltage to become zero before the controller turns the transistor on. Moreover, with a minor circuit modification, the transistor turn-off transitions can also be caused to occur at zero voltage.

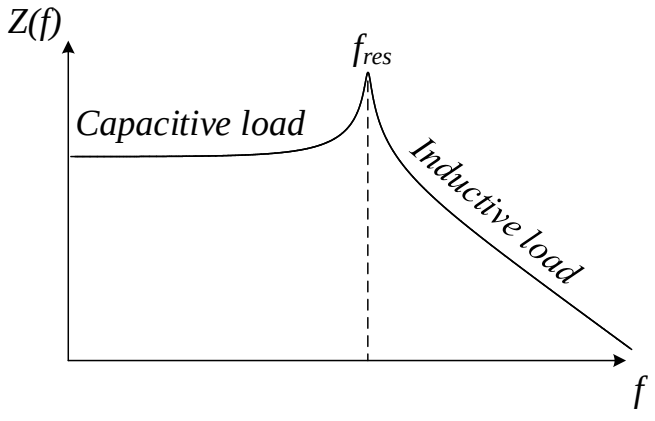

Fig. 2.13 Impedance behavior of output load in resonant tank – seperation to capacive load and nductive load, where the first is leading load and the second is lagging load.

In resonant converters that contain diodes and transistors, zero-voltage switching diminishes the switching loss otherwise caused by diode reverse recovery charge and semiconductor output capacitance. Similarly, zero-current switching can diminish the

switching loss caused by current tailing in the transistors and by stray inductances. In general, ZVS is preferred since the diode recovered charge and semiconductor output capacitances are the dominant sources of PWM switching loss.

2.4.2. Challenges of resonant converters

There are some challenges operating resonant converter that needs to be taken into consideration when designing and implementing one, as detailed below.

1. Typically, it is difficult to optimize the resonant elements such that good performance is obtained over a wide range of load currents and input voltages.
   It can be seen in Fig. 2.14 that for every different output load there is different current amplitude, which varies over range of frequencies (except of the resonant frequency where all the currents merge to the single maximum current). As a result, a certain resonant converter can be useful only for small range of load, frequency and amplitude.

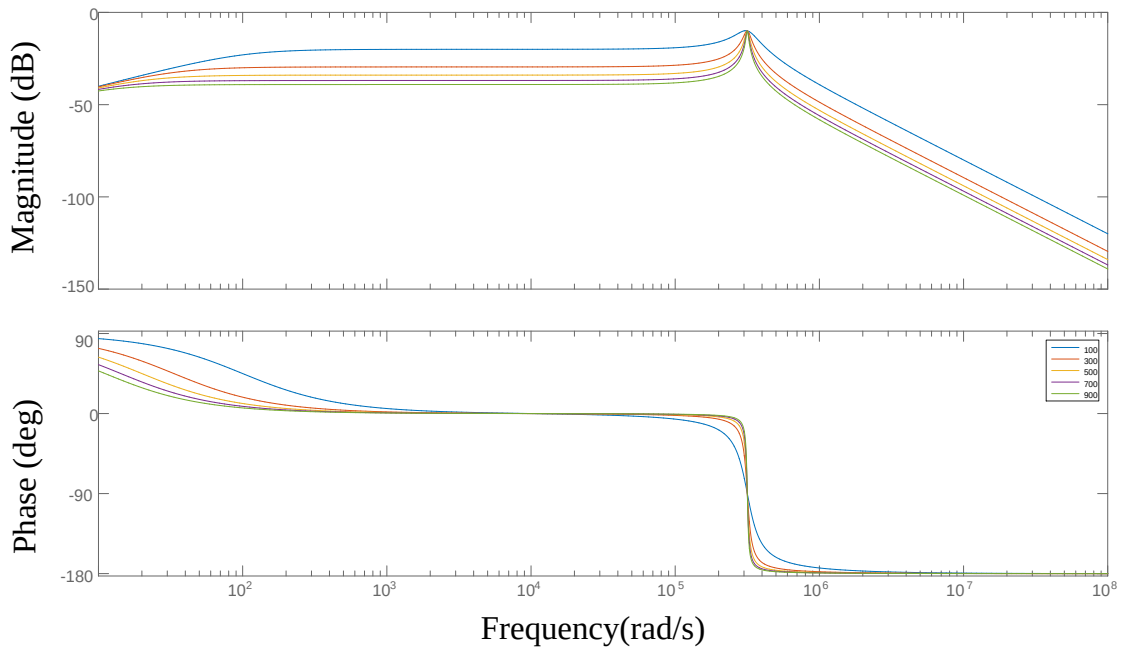

Fig. 2.14 Bode plot of the resonant currnet $I_{res}(\omega)$ for different output load R_{load}

2. Significant currents may circulate through the tank elements, even when the load is removed, leading to poor efficiency at light load. In (2.20) the connection between the output current $I_{out}(f)$ and the resonant current $I_{res}(f)$ is presented.

$$\frac{I_{out}}{I_r}(f) = \frac{1}{1+sR_lC_p} = \frac{1}{1+j\frac{fsw}{fres}Q} \qquad (2.20)$$

It can be seen that the currents ratio are a function of the quality factor Q, the switching frequency f_s and the resonant frequency f_{res}. If we desire to increase the quality factor, in order to enjoy low THD for example, then the difference between these currents increases, as can be seen in Fig. 2.15.

Similarly, the current ratio decreases when working far from the resonant frequency.

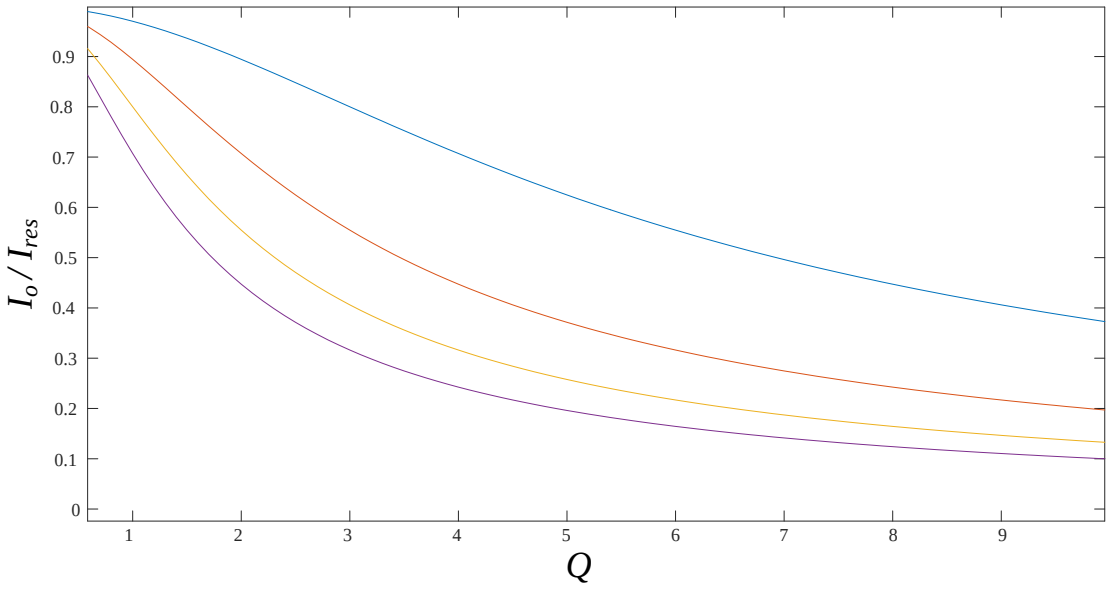

Fig. 2.15 Connection between the quality factor of the current ratio for different output load

3. Two stage current sourcing sinusoidal generator

3.1. System requirements

As discussed in the previous chapters, our research goal is to design and implement a portable sinusoidal transcutaneous muscle manipulator (Fig. 3.1), in order to apply electrical nerve block stimulation on a desired nerve.

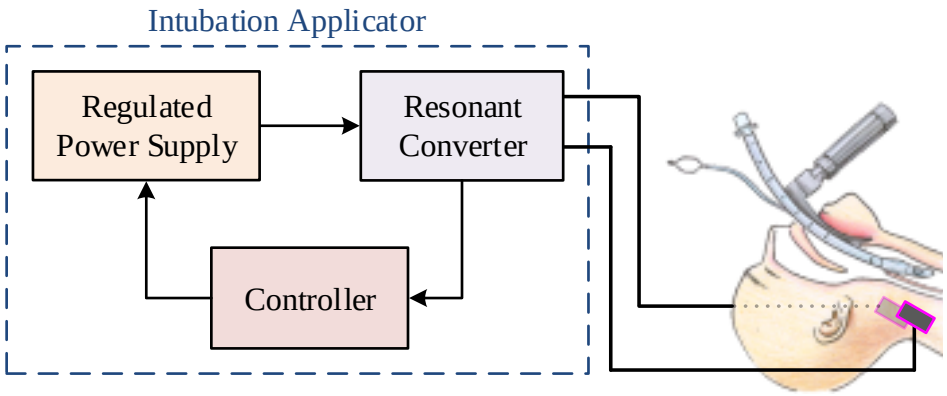

Fig. 3.1 Abstractive representation of the subject of application and the generator, builed from resonant stage, front stage and controller.

In order to achieve partial or complete nerve block, the following system requirements need to be taken in consideration while designing the system.

1. Waveform type: Biphasic AC waveforms are the common waveforms used for nerve blocking as reported and evaluated in previous literature [11].
   In particular, sinusoidal waveform was found to be the most effective nerve block stimulator, therefore it was chosen is the target waveform in this study.

2. Frequency: As mentioned in chapter 1.2, the desired frequency range in order to achieve complete nerve block is normally between 5kHz to 70kHz. As a result, the switching frequency needs to be programmable and not fixed.

3. Amplitude: Based on previous studies, discussed in chapter 1.2, there is need for adjusted output current amplitude for various degrees of paralysis..

4. Control: In order to reserve or reverse the nerve state there is a need to maintain adjusted output current amplitude, while taking into consideration the nonlinear load behavior of the human skin, as detailed in chapter 1.4.2.

For these reason, a strict control of the output current amplitude should be applied, while allowing programmable frequency, current amplitude and pulse duration.

5. Signal patterns: As mentioned in chapter 1.4.2, the sinusoidal generator should create a unique signal patterns suitable to excite nerve blocking.

3.2. Two stage sinusoidal generator

Generation of sinusoidal current waveforms can be implemented using a single resonant converter stage [43] – [49] like series or parallel resonant converter, as detailed in chapter 2.

However, when driving a nonlinear load, such as the human body, through the skin and other tissues (Fig. 1.5a), there is a challenge to maintain current amplitude as well as programmable frequency.

In addition, current requirements to relax the muscle and to maintain it relaxed are not the same. Higher current is required to initiate muscle relaxation, but once muscle relaxation is induced, much smaller amplitude current is required in order to maintain flaccid paralysis of the muscle.

To address this challenge, a functionality of programmable pattern generation, such as shown in Fig. 1.5b, is required.

To achieve sinusoidal current waveforms compliant with the goals outlined above, a two-stage topology is required [50] – [53]. The topology selected in this study consists of a first stage buck converter followed by a series-resonant parallel-loaded converter (chapter 2.3.4). The schematic of the power stage is shown in Fig. 3.2.

The buck converter adjusts the input voltage to the second stage, whereas the second stage produces high frequency alternating current. The resonant converter is in charge of generating the sinusoidal waveform at the target frequency, which is maintained to be in the vicinity and slightly above the resonant frequency in order to enjoy low THD and soft switching.

Two stage current sourcing sinusoidal generator

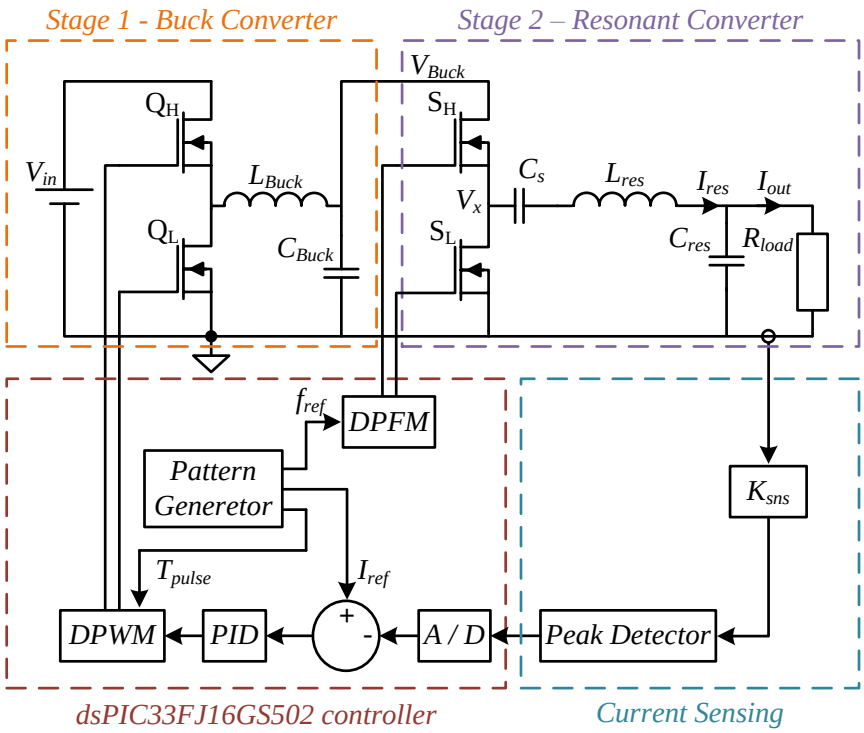

Fig. 3.2 Schematic of the two stage topology with the current sensing and control blocks.

The duty cycle of the resonant converter is designed to be equal to 50% at all time, due to the characteristics of output voltage and current constructed only from odd harmonies of sinusoidal waveform, as can be seen in (2.1). As a result, a low THD is achieved for lower quality factor.

Moreover, the resonant stage has current sourcing attributes, while the first stage buck converter tunes the output current amplitude to meet the reference current and compensates the resonant tank gain variation over the frequency range of interest.

3.3. Front stage converter

The function of the pre-regulation stage is to adjust the amplitude of the output current in the presence of wide load and input voltage variation. Input voltage variation could be due to the battery charge/discharge, while load variation comes from non-linear characteristics of the skin.

Pre-regulation stage could be DC-DC converter to provide step-up, step-down or step-up/down options depending on the source, and desired operation range. Since the prototype developed in this study has been operated of a laboratory power supply, step down buck converter was selected, as can be seen in Fig. 3.3.

Two stage current sourcing sinusoidal generator

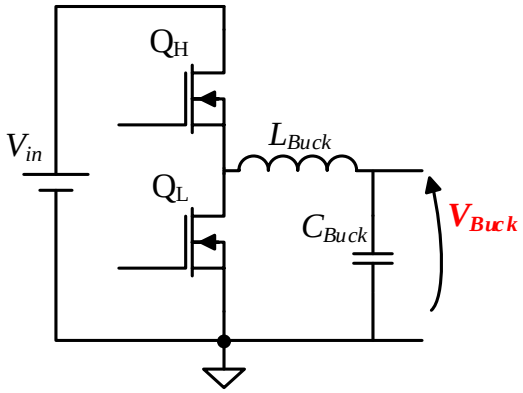

Fig. 3.3 Front stage buck converter citcuit

The impact of skin conduction on the converter loading is shown in Fig. 1.5a. For the matter of response evaluation, skin-loading behavior could be approximately modeled as a step from high impedance to low impedance load. Step from high impedance to low impedance results in a rise of the load current amplitude.

One possible option to compensate the change in output current amplitude is to shift the switching frequency and change the gain of the resonant converter. This is however, prohibitive in this application where both low THD and tight frequency control are required [22].

The alternative solution is to use pre-regulation stage to adjust the voltage fed to the resonant converter, which in turn adjusts the amplitude of the output current. PWM control is employed to adjust the output of the buck stage, and the control loop is designed to adjust the duty cycle of the buck stage as a function of the amplitude of the sinusoidal output current.

3.4. Current sensing setup

One of the options to implement current sensing of an AC signal is by using a current transformer. The benefit of this method comparing for example to a series-sense resistor [54] is the efficiency.

Current amplitudes required in this study are in the range of 1 mA to 30 mA. In order to facilitate good signal to noise ratio and to create an acceptable interface to the microcontroller's Analog to Digital Converter (ADC), the sensed current is passed through several gaining and shaping units (Fig. 3.4a).

Two stage current sourcing sinusoidal generator

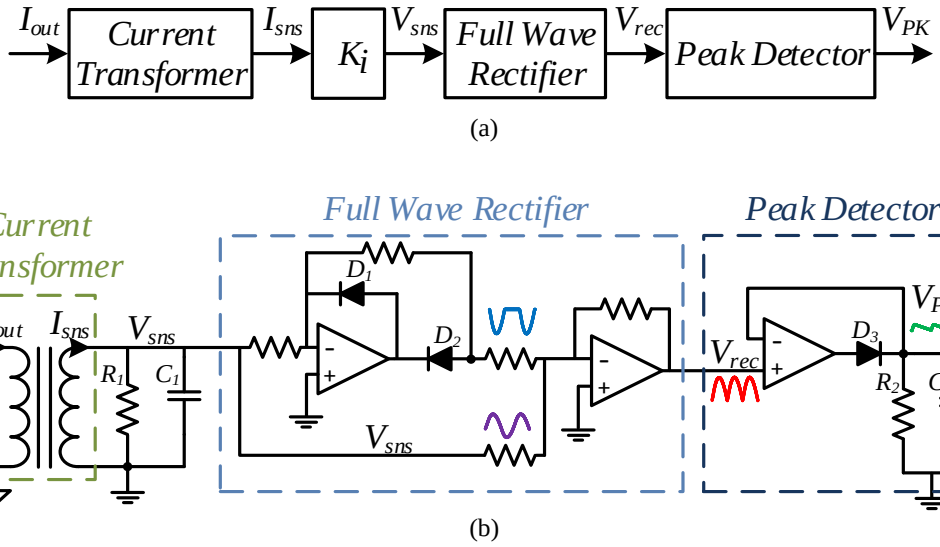

Fig. 3.4 Current sensing schematics diagram. (a) Block diagram (b) Circuit level schematics.

3.4.2. Current transformer

At the beginning, the current is passed through the current transformer itself, which is designed with high transfer ratio, 1:100 in this work. Then the current at the secondary, I_{sns} is converted into voltage by flowing through resistor R_1 (Fig. 3.4b).

It should be noted that although low current amplitudes are measured, a high attenuation current sensor is used. This is to facilitate reduced interference measurement with low power consumption.

In addition, since the output current (rather than the resonant one) is the target of this application, it is desired to add minimal amount of additional parasitic inductance to the loop. Capacitor C_1 is used to smooth the voltage waveform.

3.4.3. Wave rectifier

After the current transformer, a full wave rectifier built around operational amplifier both rectifies the sinusoidal signal and further amplifies it to match the dynamic level of MCU's built in ADC, as presented in Fig. 3.4b.

The wave rectifier is built from two stages, first stage is a half wave rectifier and the second is a summing amplifier which together construct together a full wave rectifier.

The amplifiers are fed with bipolar power supply to allow the negative input of the sinusoidal waveform. Alternatively, the potential of full wave rectifier reference and the

secondary winding of the current transformer could be raised enough above the ground to allow unidirectional operation.

3.4.4. Peak detector

Finally, in order to reduce the sampling rate requirements of the ADC, and reduce its power consumption, an analog peak detector is used.

The peak detector is implemented around operational amplifier to allow compensation of the rectifying diode D_3 voltage drop. The time constant of the peak detector is selected approximately ten times the period of the sinusoidal waveform to both, filter out the ripple, and smoothly follow the sinus peak value.

3.5. Control of two stage topology

3.5.1. Control challenge

The main control challenge in this study is associated with maintaining constant output current in the presence of wide non-linear load variation introduced mainly by the human skin (Fig. 1.5a).

The best way to address this challenge is by introducing an ideal sinusoidal current source. Resonant circuits could be treated as current sources in the immediate vicinity of their resonant frequency.

However, it is unpractical in real systems due to very high quality factor requirement, which in turn poses another challenge of locking in the operation frequency close enough to the resonant frequency. Finally, if the operation frequency needs to be adjusted on demand, than in order to maintain current source characteristics a continuously variable resonance component is required.

An alternative to ideal current source would be a controlled system that is able to regulate the frequency and the output current amplitude independently. The user has an independent freedom to change the frequency of the second stage, by adjusting the switching frequency of the resonant converter, and to adjust the output current amplitude by regulating the voltage of the first stage (Fig. 3.2).

Two stage current sourcing sinusoidal generator

3.5.2. *Two loop controller*

There two simple methods for controller implementation. First is a two loop controller, as shown in Fig. 3.5 In this case, buck converter output voltage is closed in inner loop, and resonant converter output current is closed in external red loop. This system is easy to stabilize, but it requires two control loops and additional components.

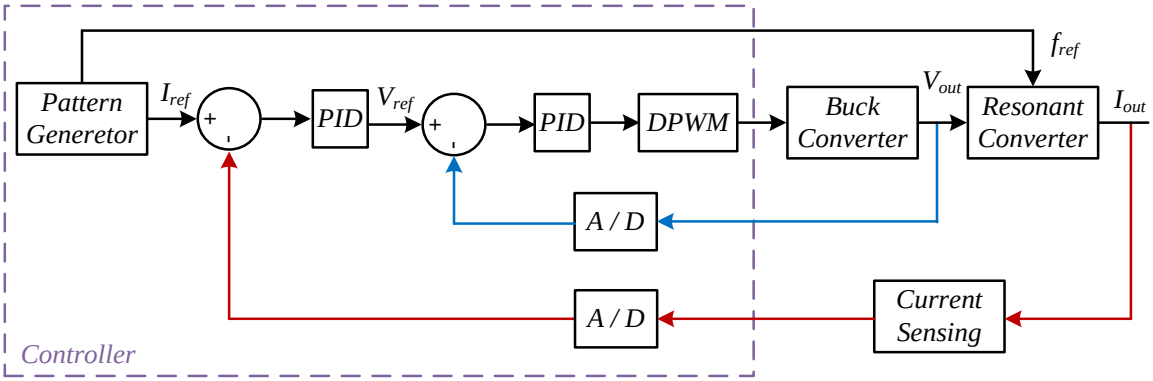

Fig. 3.5 Block diagram of two loop controller – red loop is for resonant converter output current regulation and blue loop is for buck converter output voltage regulation

3.5.3. *Single loop controller*

Another alternative approach, which was chosen in this research, is by using single loop controller, as can be seen in Fig. 3.6.

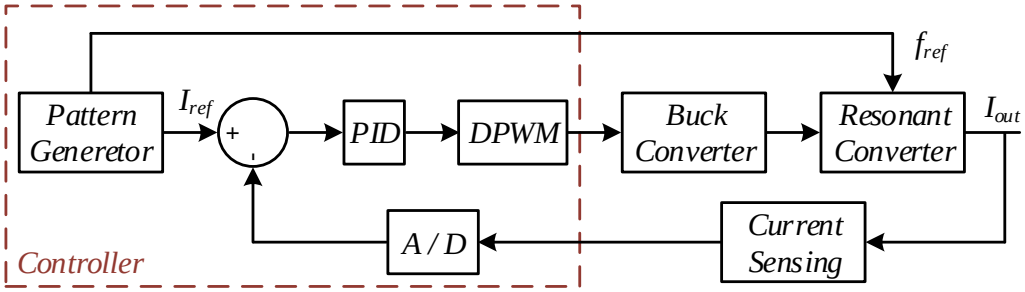

Fig. 3.6 Block diagram of single loop controller for the resonant converter output current regulation

To address the control management requirements an MCU is used. Every cycle of the resonant stage, the output voltage of the peak detector V_{PK} is sampled by the ADC.

Then, a calculation of the current error is preformed and if the error exceeds the maximum acceptable limit, a PID compensator calculates the new duty cycle D_{Buck}, which is then fed to the front-end stage. A flowchart of the algorithm is shown in Fig. 3.7.

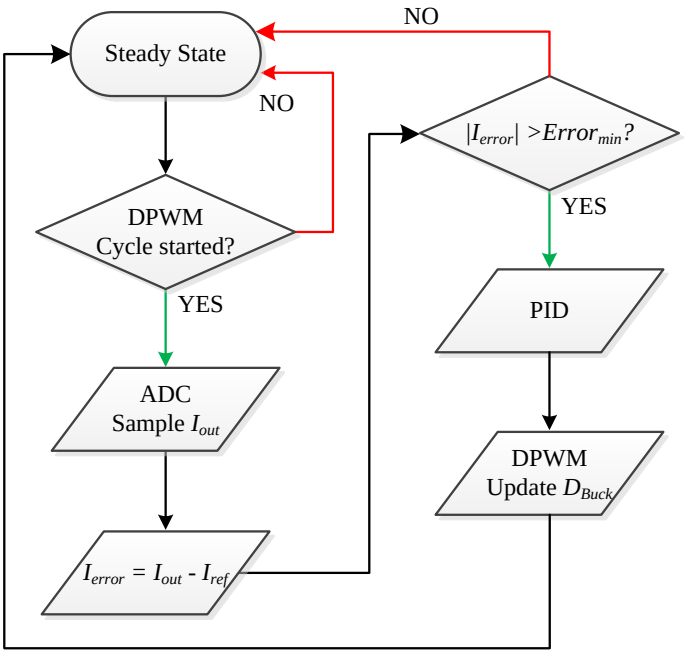

Fig. 3.7 Flow-Chart of the two-stage controller

Additional MCU function is pattern generation. The references of frequency and amplitude provided to the controller by the pattern generation block (Fig. 3.2) are varied in time to achieve certain medical functionality. In the example shown in Fig. 1.5b, first muscle relaxation is induced with higher current for short period, and then in order to hold the muscle relaxed, the current is significantly reduced and maintained for a longer period.

Moreover, the MCU provide a variation on the pulse duration of the nerve stimulation, by the user request.

4. Practical implementation

4.1. Inductance selection

The optimal operation of the resonant converter is in the inductive load range, which is above the resonance frequency of the RLC network. This range provides current sourcing behavior and enables ZVS of the main resonant converter switches, and as a result, lower losses are obtained.

The target operation-frequency range in this study is set to 5 kHz – 70 kHz, which is the most prominent range for nerve manipulation according to the medical studies [11], [14], [17] , [55].

The minimum quality factor, Q_{min} of the series-resonant parallel-loaded converter is selected according to the THD requirements. Very high quality factors however, are undesired either.

High quality factor results in a much higher reactive currents that circulate in the system, reduces system efficiency and steep transfer function that is challenging in terms of frequency and gain control. In addition, high Q results an underdamped system with long convergence time.

Therefore, the upper limit for the quality factor is limited to around 100, while the minimum quality factor has been selected to be three. To maintain the minimum quality factor, the design of the converter is carried out for the worst-case conditions, i.e. the load resistance of 100 Ω.

From the expression of the output current amplitude presented in (2.19) it can be seen that the current is a function of the input voltage and the output load.

In order to maintain constant output amplitude in the presence of wide load range a regulation of the resonant converter is used.

However, there is an additional necessity for programmable frequency over the desired range. Due to the resonant feature to operate with sufficient amplitude only for small range of frequencies, there is a need for another degree of freedom in the system.

Therefore, in this research the solution is implemented using separate inductors, L_{resn}, $n=1, 2, 3\ldots$ in order to achieve different resonant frequencies, as can be seen in Fig. 4.1.

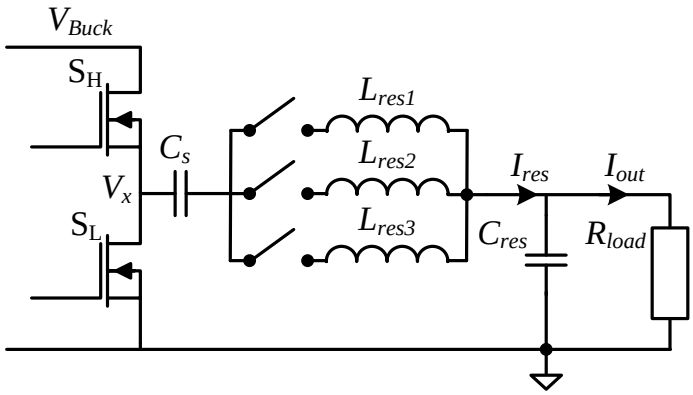

Fig. 4.1 Resonant converter schematic with three inductors for different frequency range.

Each of the inductors is chosen to cover as much frequency range as possible. An additional option to use the inductors connected in parallel is available, where the MCU is responsible to switch between the inductors, depending on the requested frequency. Bode diagram of the resonant output voltage with separate inductors, demonstrating the different possibilities, is shown in Fig. 4.2.

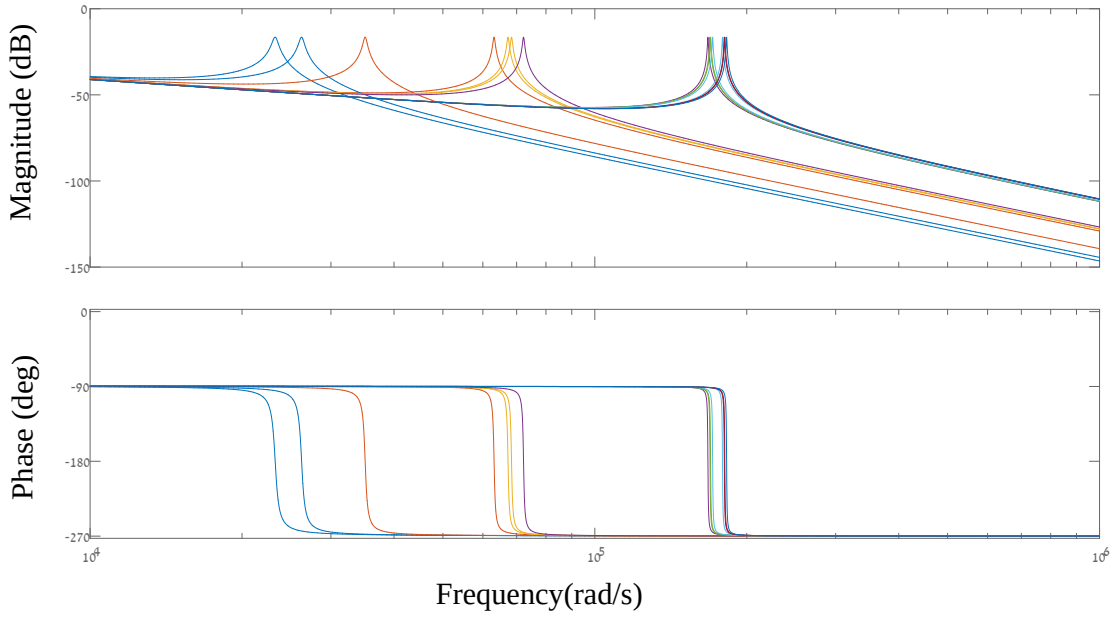

Fig. 4.2 Bode plot of the resonant output voltage $V_o(\omega)$ in case of four different inductors with all the option for parallel inductors.

For every inductor and his frequency range, the resonant frequency of the series resonant tank is selected slightly lower than the lowest expected operation frequency. Using the quality factor (2.11) and the resonant frequency (2.8) while taking into

consideration the resonant frequency and quality factor outlined above, the values of L_{res} and C_{res} are selected according to:

$$C_{res} = \frac{Q}{2\pi f_{res} R_{load}} \, , L_{res} = \frac{1}{C_{res}(2\pi f_{res})^2} \tag{4.1}$$

Resonant inductors are designed for the worst-case conditions, which is the highest expected current in the circuit.

The inductors in this circuit configuration carry larger current than the current provided to the load. The ratio between the output current $I_{out}(f)$ and the resonant inductor current $I_{res}(f)$ could be summarized in the following expression:

$$\frac{I_{out}}{I_{res}}(f) = \left| \frac{1}{1 + j \cdot (2\pi f) C_{res} R_{load}} \right| \tag{4.2}$$

Rearranging (4.2) and substituting C_{res} from (4.1), resonant current can be expressed as:

$$I_{res} = I_{out} \cdot \sqrt{1 + \left(\frac{f_{sw}}{f_{res}} \cdot Q \right)^2} \tag{4.3}$$

It follows from (4.3) that the worst-case conditions for resonant inductor, in terms of maximum resonant current, occur at the highest quality factor. This conclusion holds assuming the rest of the parameters are kept constant, such as the output current that is maintained to be constant by the buck converter, and the switching frequency, which is set to a certain frequency.

Moreover, another aspect taken into consideration when choosing system components is the voltage drop over the skin at the initiation of the system, which can be higher than needed due to control limitation. This voltage is higher when the switching frequency is far away from the resonant frequency and for high quality factor. Therefore, although needed high quality factor, there is a trade-off between the THD and the voltage drop.

4.2. Safety

An important aspect of medical devices regards to safety concerns for both the subject and the applicator. To assure that current flows on to the subject alone within the confined region of the contact electrodes, i.e., there is no electrocution hazard to the applicator, the current flow needs to be governed and monitored on both electrodes.

This can be facilitated using a single current transformer, occupying two turns on its primary, one turn from the signal line and the other from the return path, as can be seen

in Fig. 4.3. A zero-sum reading of the transformer assures that the entire current flows in the desired path without leakage.

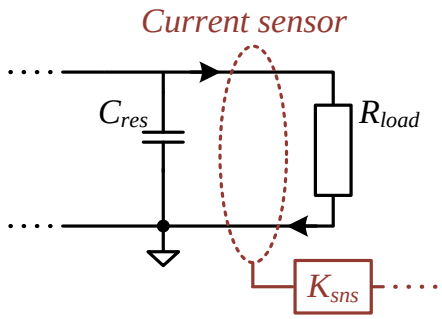

Fig. 4.3 Current sensor for output current from the single line and the return line.

It should be noted that although isolation is used in the application, parasitic capacitance leakage is still feasible, and therefore an extra measure of caution needs to be employed.

To satisfy the safety of the subject, and to prevent damage or burn of the sensitive tissues due to arching, the charge flow out of each electrode is continuously monitored, so that the application does not exceed the allowed per pulse as well as accumulative charge quantity.

4.3. Human interface

This research is conducted jointly with a team of physicians and physiologies specialize in nerve system and airway system. Although the extensive medical researche that was conducted in the last years, there is still uncertainty regarding the specific parameters required to achieve the desired flaccid paralysis.

For these reason, the system prototype that was built in this study consist many features to allow simple and comprehensive medical test.

First, there is option to modulate the main features of the system: current amplitude in 1 mA difference, resonant stage switching frequency in 1 kHz difference and pulse duration in 500 msec difference. This specific amount of research is not fixed and can be modulated by request.

Another option is a button to initiate system operation, after choosing the desired parameters for the each experiment.

5. Experimental verification

To validate and demonstrate the operation of the proposed sinusoidal generator, a laboratory prototype of two - stage resonant converter has been design and built. The converter is digitally controlled by a dsPIC33FJ16GS502 microcontroller manufactured by Microchip [56].

In order to comply with the human interface required in this application (detailed in chapter 4.3), a set of four buttons and two LEDs are added to the design, as can be seen in Fig. 5.1.

The LEDs allow the user to know which of the programmable parameters can be modified. The buttons operation is as follows:

1. Choosing parameter to change between current amplitude, resonant switching frequency and pulse duration.
2. Increasing the chosen parameter by defined quantity.
3. Decreasing the chosen parameter by defined quantity.
4. Starting the system operation for the chosen parameters.

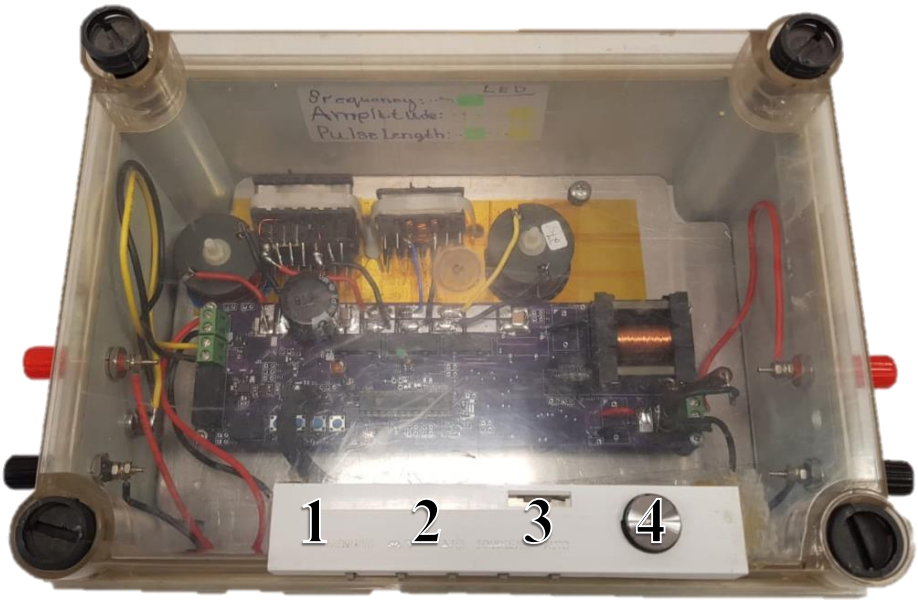

Fig. 5.1 System prototype on PCB with four buutons: starting operation, choosing parameter, increaing, decreasing and two LED for display verification.

Experimental verification

The specification of the two stage topology are summarized in two table as detailed below, TABLE I for the resonant converter parameters and TABLE II for the buck converter. It should be noted that three inductors are being used in this prototype, switched by three relays. The reason for choosing relay over MOSFET or other switches is due to their ability to operate fast for high voltages.

TABLE I. RESONANT CONVERTER PARAMETERS

Resonant Converter Component	***Value / Type***
Load resistance range	100 – 10000 Ω
Output voltage V_{out}	10V - 300V pk-pk
Frequency range f_{ref}	10 kHz - 40 kHz
Resonant capacitor C_{res}	150 nF
Resonant inductor L_{res}	14m /2mH / 180µH
Blocking capacitor C_s	1.1 µF

TABLE II. BUCK PARAMETERS

Resonant Converter Component	***Value / Type***
Input voltage V_{in}	30-90V
Output voltage V_{Buck}	0 - V_{in}
Frequency f_{Buck}	150 kHz
Buck capacitor C_{Buck}	330 µF
Buck inductor L_{Buck}	24µH

The load range of the resonant converter was chosen based on the highest expected resistance of the human skin, when initiating electrocution and the lowest expected resistance after the impedance drops to low resistance.

A typical sinusoidal current waveform of the resonant converter operation with low distortion is shown in Fig. 5.2. The Fast Fourier Transform (FFT) transformation of $I_{out}(t)$ is shown in Fig. 5.3.

The THD of the waveform in Fig. 5.3 has been calculated based on the FFT values as can be seen in (5.1),when I_{outn} is the RMS output current of the *n*th harmonic and $n=1$ is fist harmony in the fundamental frequency. It was found to be 2%, as desired in this application.

$$THD = \frac{\sqrt{I_{out2}^2 + I_{out3}^2 + I_{out4}^2 + \cdots + I_{outn}^2}}{I_{out1}} \quad (5.1)$$

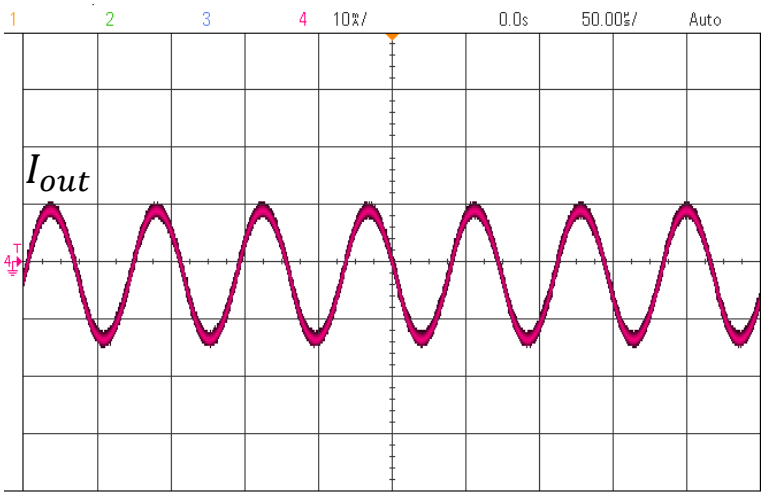

Fig. 5.2 Converter operation on time domain - sinusoidal output current, *Iout* (10mA/div), Horizontal axis (500us/div)

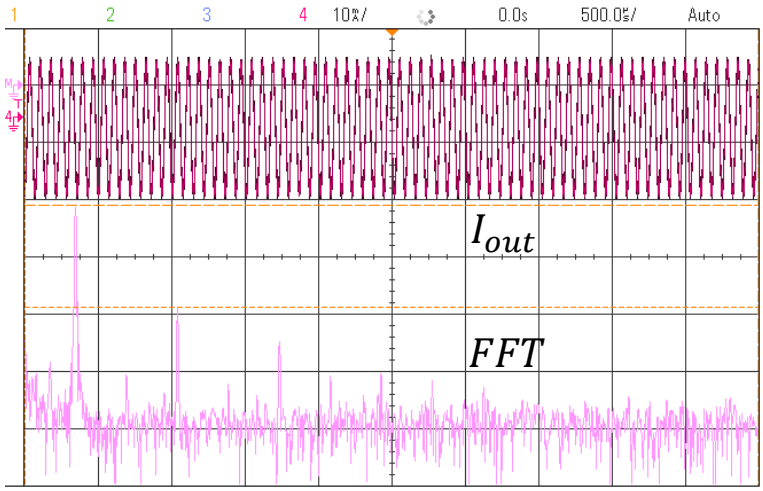

Fig. 5.3 FFT of the output current, Top trace (red) – Output current I_{out} (10mA/div), Horizontal axis (500us/div); Bottom trace (pink) – FFT of the output current (20dB/div), Horizontal axis (20kHz/div);

The system's response to load changes is demonstrated in Fig. 5.4. A step from light load 1 kΩ to heavy load 100 Ω, i.e. the condition of high initial resistance of the skin that is reduced after the conduction is initiated is shown in Fig. 5.4a.

The system adjusts to the reference output current in less than 2 ms, which is approximately 30 switching cycles of 14 kHz sinusoidal waveform, and is approximately the quality factor of the circuit at these conditions. An opposite step from heavy load of 100 Ω to the light load of 1 kΩ is shown in Fig. 5.4b.

It should be noted that in order to achieve a virtually pure sinusoidal output current, the system has very high quality factor, hence, the relatively long convergence time of the waveform.

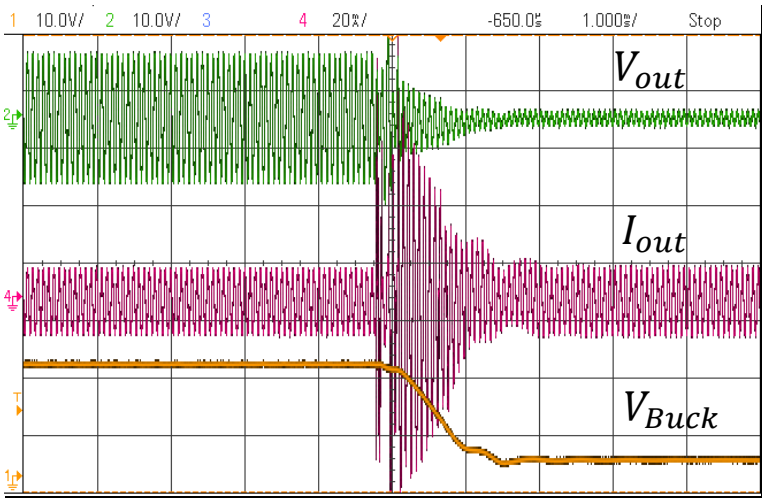

(a)

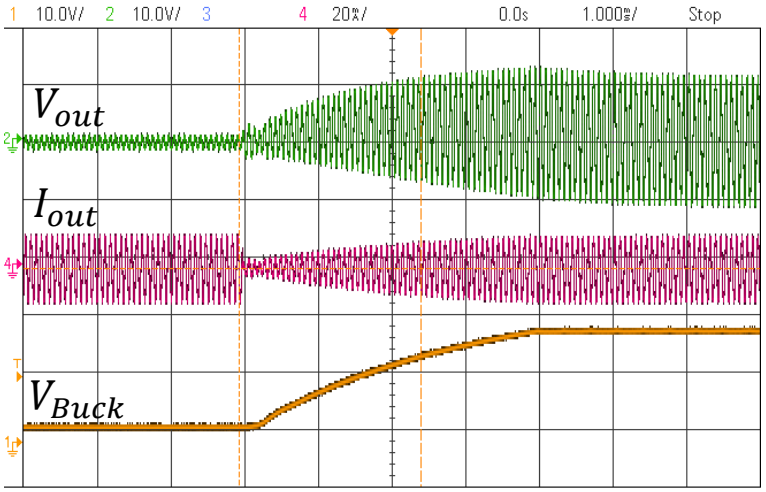

(b)

Fig. 5.4 Load change compensation: (a) 1000[Ω] to 100[Ω]. (b) 100[Ω] to 1000[Ω]. Top trace (green) – Output voltage V_{out} (10V/div). Middle trace (red)– Output current I_{out} (20mA/div). Bottom trace (yellow) – Input voltage of the second stage V_{Buck} (10V/div)

Current pattern generation capability is shown in Fig. 5.5. Current pattern that was discussed in Fig. 1.5 that requires higher current for short period to induce muscle relaxation, and then much lower current to maintain muscle relaxation is shown in Fig. 5.5a, repeated at 6Hz. Additional pattern with three different amplitudes and time periods is shown in Fig. 5.5b.

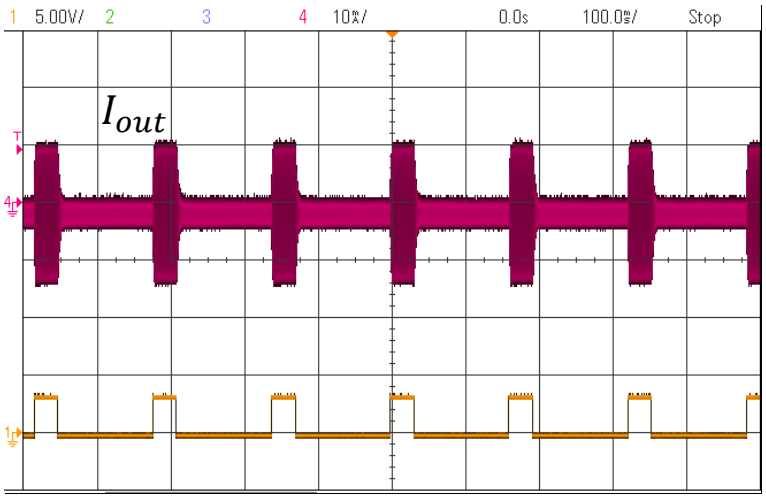

(a)

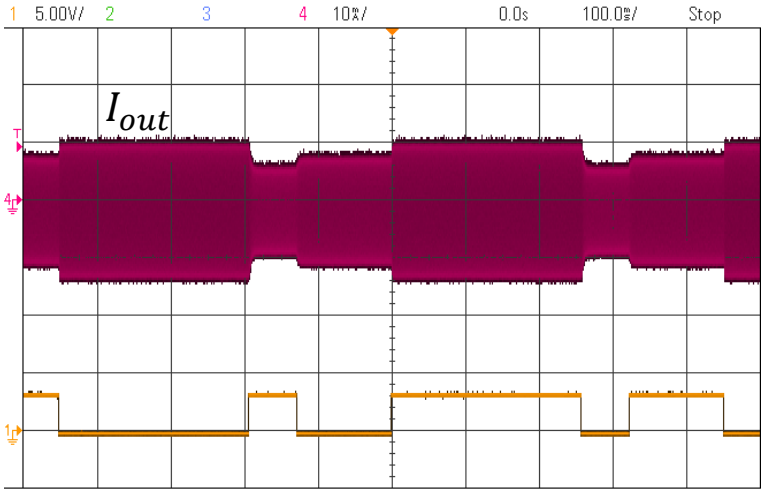

(b)

Fig. 5.5 Pattern generation - changing current amplitude. Top trace (red) – Output current I_{out} (10mA/div). Bottom trace (yellow) – pattern synchronization signal.

An experiment with a non-linear load, bringing the load behavior as close as possible to the behavior of the skin and tissues around the neck was carried out.

For this purpose a pattern of pulse bursts, where the pulse output is toggled between on and off state was generated, and the load was varied from burst to burst.

Load variation was carried out by initially connecting a 10kΩ resistor to the output, and then one of the experimenters was touching with his hand the application electrodes, connected to the output in parallel to the resistor, as can be seen in Fig. 5.6.

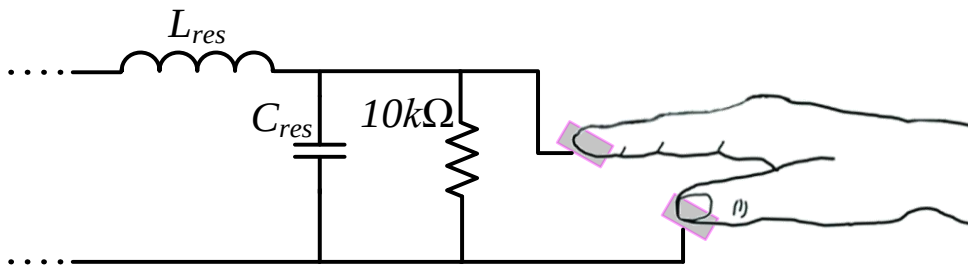

Fig. 5.6 Experimental setup for non-linear load change.

The resulting non-linear change in total resistance of the load could be tracked by the system response in Fig. 5.7.

In Fig. 5.7a an experiment with a decrease in the output resistance is shown, i.e. the experimenter is touching the electrodes approximately after 3 horizontal divisions (at 60ms).

As a result, buck output voltage (green trace) and the amplitude of the output voltage (yellow/brown trace) begin to decrease, while the amplitude of the output current is maintained constant, within the bandwidth limitations of the controller.

In Fig. 5.7b an experiment with an increase in the output resistance is shown, where the experimenter holds the electrodes at the beginning, and releases them at approximately 100-110ms.

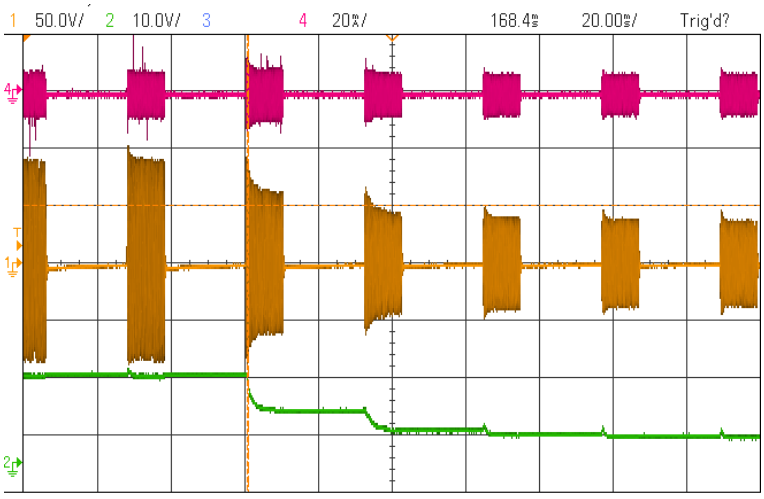

(a)

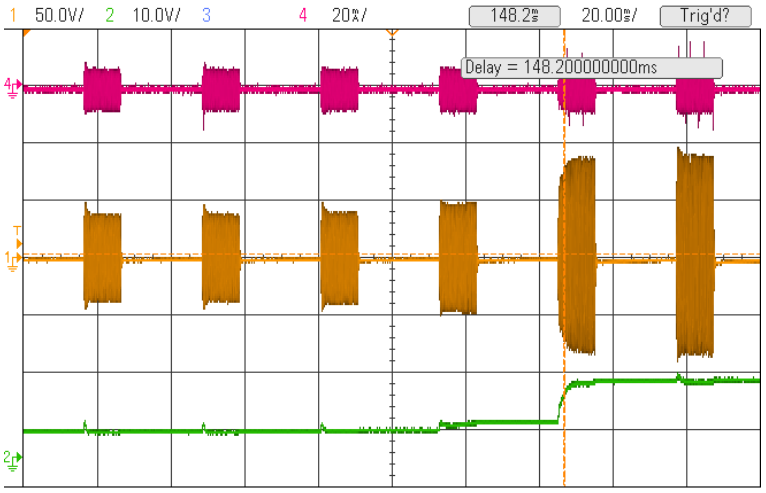

(b)

Fig. 5.7 Non-linear load change during burst generation. (a) Load increase (resistance decrease); (b) Load decrease (resistance increase).

As a result, buck output voltage (green trace) and the amplitude of the output voltage (yellow / brown trace) begin to increase. As in the previous case the amplitude of the output current is maintained constant by the system, achieving a behavior of nearly ideal current source.

To evaluate the system response to non-linear load application during a single burst of pulses, a 20ms burst was generated, and an experimenter touching of the electrodes was timed to coincide with approximately the beginning of the burst.

The resulting system response is shown in Fig. 5.8. It can be seen that during the first 10ms after the beginning of the pulses burst, and the application of the non-linear load, the system carries out a series of corrections to maintain the current constant.

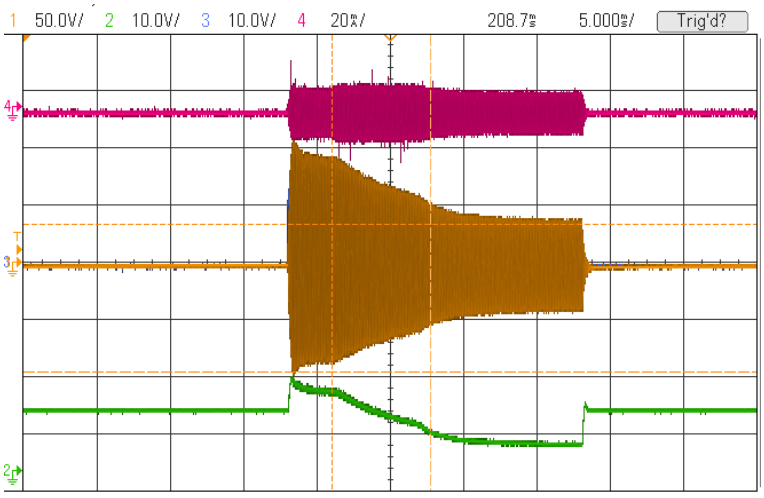

Fig. 5.8 Non-linear load change during a single burst of pulses. Load increased and resistance decreased.

Despite a slight increase in the output current as a response to the load, which is due to the limitations of the controller bandwidth, overall current amplitude is maintained very close to the reference value during the load variation period.

Another observation from Fig. 5.8 is the non-linear practical response of the skin and the tissue, which is due to the constant current maintained by the system, could be derived from the buck output voltage (green trace).

6. Discussion

6.1. Contribution of the research

The key contributions of this work are summarized as follows:

Noninvasive approach for overcoming airway obstruction – As oppose to standard electrical nerve excitation that are being used nowadays, the suggested solution in this research offers transcutaneous muscle manipulation using external electrodes to deliver the desired waveform. This solution is not only non-invasive by its nature but also allows operation in critical medical states as well as in routine procedures.

Design procedure for two stage resonant converter – Following the system requirements for programmable frequency, amplitude and time duration while creating unique signal patterns, a two-stage resonant converter has been carried out, detailing control and current sensing approach. The design presents an attractive alternative for electrical nerve excitation application.

Full design of power stage – including safety aspect and human interface – A two-stage current sourcing sinusoidal generator has been designed and implemented on PCB. The system consist tight control and various features to allow simple verification and modulation of the significant parameters. Moreover, the charge flow out of each electrode is continuously monitored to verify safety of the subject. In addition, the system features option to modulate on real time operation several system parameters to comply with human interface.

Design guidelines and preliminary experimental results of two stage sinusoidal generator – This study introduces a preliminary prototype of current sourcing generator. The system was tested for load changes response, to simulate as close as possible to the human skin behavior, in both continuance time and during a single burst of pulses. Moreover, an experiment on skin was made using external electrodes.

6.2. Suggestions for future research

Some suggestions for future lines of investigation that can be developed as a result of this thesis are outlined below:

Extend the research for various AC currents waveforms – Although sinusoidal waveform was found to be the most promising option to achieve flaccid paralysis, there is an interest to investigate other AC waveform, such as rectangular, bipolar pulse and so on, and there influence on the airway nerves. Therefore, there is a need to adjust the system to supply the various wave while allowing the programmable parameters as well.

Diminish required range of output current amplitude, switching frequency and time duration –The following step after analyzing the results of the current system should include more precise information about the desired parameters of the system, in order to achieve flaccid paralysis. By doing so, the system size will be diminished and the controller implementation would be simpler.

7. References

[1] H. P. Habany, M. Evzelman and M. M. Peretz, "Signal and Pattern Generation for Muscle Manipulation in Medical Applications," *2019 IEEE Applied Power Electronics Conference and Exposition (APEC)*, Anaheim, CA, USA, 2019, pp. 701-707.

[2] A. A. Alalami, C. M. Ayoub, A. S. Baraka, "Laryngospasm: Review of different prevention and treatment modalities", *Paediatr Anaesth*, vol. 18, issue 4, pp.281–288, 2008.

[3] L. Steven, M. D. Orebaugh "Succinylcholine: Adverse Effects and Alternatives in Emergency Medicine", *The American journal of emergency medicine*, 1999

[4] R. C. Sinclair, M.C Luxton, "Rapid sequence induction" *Continuing Education in Anaesthesia, Critical Care & Pain* 5.2 pp. 45-48, 2005.

[5] L. Nel, E. Eren, "Peri-operative anaphylaxis", *BJCP Special Issue: Drug allergy: themed section*, vol. 71, issue 5 pp. 647-658, 2011.

[6] G. Kovacs, J. A. Law, *Airway management in emergencies*, USA PMPH, 2011.

[7] Hambrecht, F.T, "Functional electrical stimulation: an overview." *Pacing and Clinical Electrophysiology* vol. 12, issue 5, pp. 840-843, 1989.

[8] N. Bhadra, T. L. Vrabec, N. Bhadra, and K.L. Kilgore, "Reversible conduction block in peripheral nerve using electrical waveforms" *Bioelectronics in medicine* vol.1, no. 1, pp. 39-54, 2017.

[9] Y. A. Patel, B. S. Kim, W. S. Rountree and R. J. Butera, "Kilohertz Electrical Stimulation Nerve Conduction Block: Effects of Electrode Surface Area," in *IEEE Transactions on Neural Systems and Rehabilitation Engineering*, vol. 25, no. 10, pp. 1906-1916, Oct. 2017.

[10] L. Bugnard, A.V. Hill. "High-frequency stimulation of nerve and the refractory period." *J. Physiol* , pp. 383-393, 1935.

[11] K. L. Kilgore and N. Bhadra, "Nerve conduction block utilising high frequency alternating current," *Med. Biol. Eng. Compute.*, vol. 42, no. 3, pp. 394–406, May 2004.

[12] L. Joseph and R. J. Butera, "High-frequency stimulation selectively blocks different types of fibers in frog sciatic nerve," *IEEE Trans. Neural Syst. Rehabil. Eng*., vol. 19, no. 5, pp. 550–557, Oct. 2011.

[13] J. A. Tanner, "Reversible blocking of nerve conduction by alternating-current excitation." *Nature* pp. 712-713, 1962.

[14] Y. A. Patel and R. J. Butera, "Differential fiber-specific block of nerve conduction in mammalian peripheral nerves using kilohertz electrical stimulation," J. *Neurophysiol*., vol. 113, no. 10, pp. 3923–3929, 2015.

[15] R. P. Williamson and B. J. Andrews, "Localized electrical nerve blocking," *IEEE Trans. Biomed. Eng.*, vol. 52, no.3, pp. 362–370, Mar. 2005.

[16] N. Bhadra and K. L. Kilgore, "Block of mammalian motor nerve conduction using high frequency alternating current," *Proc. 2nd Int. IEEE EMBS Conf. Neural Eng*., vol. 10. Mar. 2005, pp. 1–3.

[17] N. Bhadra, N. Bhadra, K. Kilgore, and K. J. Gustafson, "High frequency electrical conduction block of the pudendal nerve," *Journal of Neural Engineering*, vol. 3, no. 2, pp. 180–187, 2006.

[18] A. Boger, N. Bhadra, and K. J. Gustafson, "Different clinical electrodes achieve similar electrical nerve conduction block," *J. Neural Eng*., vol. 10, no. 5, p. 056016, 2013.

[19] E. Lin, K. L. Kilgore, N. Bhadra, and E. A. Lahowetz, "Chronic high frequency nerve block with an implanted waveform generator," *Proc. Int. Funct. Elect. Stimulation Soc. Conf*., 2007.

[20] J. M. Cuellar, K. Alataris, A. Walker, D. C. Yeomans, and J. F. Antognini, "Effect of high-frequency alternating current on spinal afferent nociceptive transmission," *Neuromodulation, Technol. Neural Interface*, vol. 16, no. 4, pp. 318–327, 2013.

[21] M. Camilleri., "Intra-abdominal vagal blocking (VBLOC therapy): Clinical results with a new implantable medical device," *Surgery*, vol. 143, no. 6, pp. 723–731, 2008.

[22] K. L. Kilgore and N. Bhadra. "Reversible nerve conduction block using kilohertz frequency alternating current," *Neuromodulation: Technology at the Neural Interface*, vol.17, issue 3, pp. 242-255, 2014.

References

[23] L. Joseph and R. J. Butera, “Unmyelinated Aplysia nerves exhibit a non-monotonic blocking response to high-frequency stimulation,” *IEEE Trans. Neural Syst. Rehabil. Eng.*, vol. 17, no. 6, pp. 537–544, Dec. 2009.

[24] C. Tai, D. Guo, J.Wang, J. R. Roppolo, and W. C. de Groat, “Mechanism of conduction block in amphibian myelinated axon induced by biphasic electrical current at ultra-high frequency,” *Journal of computational neuroscience,*, vol. 31,no. 3, pp. 615–623, Nov. 2011.

[25] N. Bhadra and K. L. Kilgore, “High-frequency electrical conduction block of mammalian peripheral motor nerve,” *Muscle Nerve*, vol. 32, no. 6, pp. 782–790, Dec. 2005.

[26] M. C. Bicket, R. Y. Dunn, and S. U. Ahmed, “High-frequency spinal cord stimulation for chronic pain: Pre-clinical overview and systematic review of controlled trials,” *Pain Med.*, vol. 17, no. 12, pp. 2326–2336, 2016.

[27] D. M. Ackermann, Jr., N. Bhadra, E. L. Foldes, X. F. Wang, and K. L. Kilgore, “Effect of nerve cuff electrode geometry on onset response firing in high-frequency nerve conduction block,” *IEEE Trans. Neural Syst. Rehabil. Eng.*, vol. 18, no. 6, pp. 658–665, Dec. 2010.

[28] D. M. Ackermann, Jr., E. L. Foldes, N. Bhadra, and K. L. Kilgore, “Effect of bipolar cuff electrode design on block thresholds in high frequency electrical neural conduction block,” *IEEE Trans. Neural Syst. Rehabil. Eng.*, vol. 17, no. 5, pp. 469–477, Oct. 2009.

[29] E. L. Foldes, D. M. Ackermann, N. Bhadra and K. L. Kilgore, "Counted cycles method to quantify the onset response in high-frequency peripheral nerve block," *2009 Annual International Conference of the IEEE Engineering in Medicine and Biology Society*, Minneapolis, MN, 2009, pp. 614-617.

[30] Reilly, J. Patrick, Applied bioelectricity: from electrical stimulation to electropathology, Springer Science & Business Media, 2012.

[31] R. P. Severns and G Bloom, “Modern DC-to-DC Switch mode Power Converter Circuits”, New York: Van Nostrand Reinhold, 1985.

[32] J. G Kassakian, M. S. Schlecht, and G C. Verghese, “Principles of Power Electronics”, Reading, MA: Addison-Wesley, 1991.

[33] N. Mohan, T. M. Undeland, and W. P. Robbins, “Power Electronics: Converters, Applications and Design”, 3rd Ed.

[34] R. W. Erickson and D. Maksimovid, “Fundamentals of Power Electronics”, 2nd Ed. Norwall, MA: Kluwer Academic, 2001.

[35] I. Batarseh, Power Electronic Circuits, Hoboken, NJ: John Wiley & Sons, 2004.

[36] A. Carlosena, P. Martinez and S. Porta, "Wein-bridge oscillators with opamp independent oscillation frequency," in *IEEE Transactions on Instrumentation and Measurement*, vol. 40, no. 3, pp. 644-646, June 1991.

[37] G. Gonzalez, *Foundations of oscillator circuit design*, Norwood: Artech House, 2007.

[38] E. Villanueva, P. Correa, J. Rodriguez and M. Pacas, "Control of a Single-Phase Cascaded H-Bridge Multilevel Inverter for Grid-Connected Photovoltaic Systems," in *IEEE Transactions on Industrial Electronics*, vol. 56, no. 11, pp. 4399-4406, Nov. 2009.

[39] M. K. Kazimierczuk, D. Czarkowski, *Resonant power converters*, John Wiley & Sons, 2012.

[40] R. W. Erickson, and D. Maksimovic, Fundamentals of power electronics. *Springer Science & Business Media*, 2007.

[41] M. C. Cosby and R. M. Nelms, "Designing a parallel-loaded resonant inverter for an electronic ballast using the fundamental approximation," *Proceedings Eighth Annual Applied Power Electronics Conference and Exposition,*, San Diego, CA, USA, 1993, pp. 418-423.

[42] S. Ben-Yaakov, M. M. Peretz, J. M. Parra and J. M. Parra, "Self-Oscillating Constant-Current Fluorescent Lamp Driver: Theory and Application," *2007 IEEE Power Electronics Specialists Conference*, Orlando, FL, 2007, pp. 3093-3099.

[43] J. Hong, D. M. Vilathgamuwa, N. Ghasemi, T. Ishrat, and J. You, "A single phase DC-AC dual active bridge series resonant converter for photovoltaic applications," *IEEE 12th International Conference on Power Electronics and Drive Systems (PEDS)*, pp. 881-886, Honolulu, HI, 2017

[44] Y. Jang and M. M. Jovanovic, "Constant-frequency resonant inverter for AC-bus distribution system," *Twentieth Annual IEEE Applied Power Electronics Conference and Exposition. APEC 2005*, Austin, TX, 2005, pp. 864-870 Vol. 2.

References

[45] Y. A. Ang, D. Stone, C. Bingham and M. Foster, "Rapid Analysis & Design Methodologies of High-Frequency LCLC Resonant Inverter as Electrodeless Fluorescent Lamp Ballast," *2007 IEEE 7th International Conference on Power Electronics and Drive Systems*, Bangkok, pp. 139-144, 2007.

[46] H. L. Li, A. Hu and G. A. Covic, "Development of a discrete energy injection inverter for contactless power transfer," *3rd IEEE Conference on Industrial Electronics and Applications*, Singapore, pp. 1757-1761, 2008.

[47] B. Dobrucky, M. Prazenica, S. Kascak and J. Kassa, "HF link LCTLC resonant converter with LF AC output," 38th Annual Conference on IEEE Industrial Electronics Society, Montreal, QC, pp. 447-452, 2012.

[48] S. Ben-Yaakov, M. M. Peretz, J. M. Parra, and J. M. Parra, "Self-Oscillating Constant-Current Fluorescent Lamp Driver: Theory and Application," *IEEE Power Electronics Specialists Conference*, Orlando, FL, pp. 3093-3099, 2007.

[49] G. C. Hsieh and C. M. Wang, "One-cycle controlled half-bridge series-resonant DC to AC inverter with reduced conduction loss," *IEEE Industrial Electronics, Control and Instrumentation*, 1997.23rd International Conference on, New Orleans, LA, vol.2, pp. 786-791, 1997.

[50] M. Evzelman, H. Wang, R. Zane and X. Zhao, "Two-stage sinusoidal generator with calibration and pulse train amplitude feedback for ultrasonic applications," *2017 IEEE Applied Power Electronics Conference and Exposition (APEC)*, Tampa, FL, pp. 2124-2130, 2017.

[51] F. J. Ferrero, M. Rico, J. M. Alonso, C. Blanco, M. Gonzalez and J. C. Campo, "A unity power factor electronic ballast for HPS lamps, resonant current controlled," *Conference Record of 1998 IEEE Industry Applications Conference. Thirty-Third IAS Annual Meeting*, St. Louis, MO, USA, vol.3, pp. 2122-2129, 1998.

[52] J. M. Correa, E. D. Hutto, F. A. Farret and M. G. Simoes, "A fuzzy-controlled pulse density modulation strategy for a series resonant inverter with wide load range," *Power Electronics Specialist Conference*, 2003. PESC '03. IEEE 34th Annual, vol.4, pp. 1650-1655, 2003.

[53] M. N. Kim, Y. S. Noh, J. G. Kim, T. W. Lee and C. Y. Won, "A new active power decoupling using Bi-directional Resonant Converter for flyback-type AC-module system," *2012 IEEE Vehicle Power and Propulsion Conference*, Seoul, pp. 1333-1337, 2012.

[54] H. P. Forghani-zadeh and G. A. Rincon-Mora, "Current-sensing techniques for DC-DC converters," *2002 IEEE 45th Midwest Symposium on Circuits and Systems (MWSCAS)*, vol. 2, pp. 577-580, 2002.

[55] N. Bhadra, E. Foldes, T. Vrabec, K. Kilgore, and N. Bhadra, "Temporary persistence of conduction block after prolonged kilohertz frequency alternating current on rat sciatic nerve," *Journal of neural engineering*, vol. 15, num. 1, 2018.

[56] Microchip Technology, Inc., "16-bit digital signal controllers with high speed PWM, ADC, and comparators," DS70000318G datasheet, 2008. [Revised May 2014].

תקציר

עבודה זו עוסקת ביצירת אותות ודפוסים עבור מניפולציית שרירים דרך העור בשביל אפליקציות רפואיות. העבודה מתמקדת בעיקר בקשיים בדרכי הנשימה, בעיה אשר מסכנת חיים עקב חסימת נתיב אוויר ונפתרת כיום לרוב על ידי אמצעים לא חשמליים בעלי חיסרון משמעותי של מהירות פעולה. המטרה העיקרית של עבודה זו היא לתכנן וליישם מחולל זרם סינוסואידלי נישא בעל דפוסי אותות המסוגלים להרפות את השריר האחראי על נתיב הנשימה ולהשאיר את השריר רפוי עבור משך זמן הנדרש לביצוע התהליך, כל זאת תוך שמירה על עבודה בטוחה הן עבור המפעיל והן עבור המטופל לאורך כל הזמן הנתון.

אחת המטרות של עבודה זו היא להציג מחולל זרם סינוסואידלי עבור אפליקציות של מניפולציות שרירים. באפליקציות של עירור עצב ע"י חשמול הזרם עובר דרך אלקטרודות המקיפות את העצב, שיטה פולשנית ולא מעשית במקרה של טראומה וחסימת נתיב אוויר.לכן, על ידי הפעלת מכשיר המבצע מניפולציית שרירים דרך העור, ניתן להחליף את האלקטרודות מקיפות העצב באלקטרודות חיצוניות המונחות על העור. המכשיר יכול להיות בשימוש גם במצבים מסכני חיים וגם בפרוצדורות רפואיות שגרתיות. על מנת להשיג מטרה זו, בעבודה זו מוצגות שתי דרגות של ממיר זרם סינוסואידלי אשר דוחף עומס לא לינארי, בדומה לדחיפת עומס גוף האדם דרך העור והרקמות השונות. המחקר מכיל הקדמה על עירור חשמלי של עצב והאתגרים בהפעלת המכשיר דרך העור, פרטים אודות הארכיטקטורה של המערכת, עקרון העבודה של ממיר תהודתי ושתי דרגות ממיר תהודתי, גישת חישת זרם המוצא, אלגוריתם בקרת המערכת, יישומים מעשיים, ממשק אנושי, התייחסות לנושא הבטיחות ותוצאות ניסוייות של אב טיפוס ראשוני של המערכת שנבנה ונבדק.

מטרה נוספת של עבודה זו היא יצירת דפוסי אותות ייחודיים המתאימים לעירור חשמלי של העצב וחסימת פעולתו באופן מהיר וניתן לשינוי. עקב אי ודאות בנושא הפרמטרים המדויקים הדרושים להשגת השיתוק הזמני הרצוי, המכשיר מכיל אפשרויות נפרדות של שינוי אמפליטודת זרם המוצא, משך זמן הפעולה ותדר מיתוג המערכת.

רוב המחקר פורסם כמאמר בכנס - IEEE Applied Power Electronics Conference and Exposition (APEC) 2019 [1].

אוניברסיטת בן-גוריון בנגב
הפקולטה למדעי ההנדסה
המחלקה להנדסת חשמל ומחשבים

יצירת אותות ודפוסים עבור מניפולציות שרירים באפליקציות רפואיות

חיבור זה מהווה חלק מהדרישות לקבלת תואר מגיסטר בהנדסה

מאת: חגית פרץ חבני

מנחה:

פרופ' מור מרדכי פרץ

המחבר: חגית פרץ חבני ..... תאריך: 06.10.19

מנחה: פרופ' מור מרדכי פ. ..... תאריך: 06.10.19

יו"ר ועדת הוראה לתואר שני:

שם: .... תאריך: 04.02.2020

אוניברסיטת בן-גוריון בנגב
הפקולטה למדעי ההנדסה
המחלקה להנדסת חשמל ומחשבים

יצירת אותות ודפוסים עבור מניפולציות שרירים באפליקציות רפואיות

חיבור זה מהווה חלק מהדרישות לקבלת תואר מגיסטר בהנדסה

מאת: חגית פרץ חבני

מנחה:

פרופ' מור מרדכי פרץ